Modeling and Performance Analysis of Multitaper Detection Using Phase-Type Distributions over MIMO Fading Channels

Modeling and Performance Analysis of Multitaper Detection Using Phase-Type Distributions over MIMO Fading Channels

Ebtihal H. G. Yousif[1], *Member, IEEE,* and Tharmalingam Ratnarajah[1], *Senior Member, IEEE* and Mathini Sellathurai[2], *Senior Member, IEEE*

Abstract

This paper presents modeling and analysis of two variations of the multitaper detector namely multiple antenna detection of a single-user multiple-input-multiple-output (MIMO) node, and the multitaper method (MTM) combined with singular value decomposition (SVD), which is known as the MTM-SVD processor. Motivated by the reputation of the MTM as the best nonparametric power spectral density (PSD) estimator and after reviewing the limited previous research attempts, which focus on single-input-single-output (SISO) multitapering, we present the exact analytical models for the two considered derivatives of the multitaper method over fading channels by making use of the theory of Hermitian forms and Phase-Type distributions. In addition, using the Neyman-Pearson Approach (NPA), the performance of both detectors is optimized over Nakagami fading. For both multitaper variations, we accurately derive the eigenvalues of the Hermitian form of each detector, where the eigenvalues identify the Phase-Type distribution parameters. This yields generalized expressions for the probabilities of false alarm and missed detection when arbitrary multitaper weights are used. Finally, we investigate the impact of noise uncertainty on the performance of MIMO-MTM. The results show that performance of both detectors is dependent on the total number of discrete prolate spheriodal sequences (DPSSs), while for the MTM-SVD processor the performance is also dependent on the number of cooperating users and the employed frequency resolution. It is also shown that MIMO-MTM is robust under noise uncertainty. The obtained analytical models are proven to be accurate and enables further investigations on the multitaper detector.

Index Terms

Cognitive Radio (CR), Eigenvalue Analysis, Hermitian forms, Hypoexponential distribution, Multitaper Estimator, Phase-Type distributions, Spectrum sensing.

[1]Ebtihal Yousif and Tharmalingam Ratnarajah are with the Institute of Digital Communication (IDCOM), School of Engineering, The University of Edinburgh, Edinburgh, UK, e-mails: e.yousif@ed.ac.uk, t.ratnarajah@ed.ac.uk.

[2]Mathani Sellathurai is with the School of Engineering and Physical Sciences, Heriot-Watt University, Edinburgh, UK, e-mail: M.Sellathurai@hw.ac.uk

This work is supported by the Seventh Framework Programme for Research of the European Commission under grant number ADEL-619647.

I. Introduction

A. Background

The rapid growth of the commercial wireless communication services, along with the foreseen inefficiency of the current spectrum management policies, have led to a massive demand for flexible spectrum handling strategies. Hence, based on the software defined radio (SDR) platform, the concept of cognitive radios (CRs) was introduced by Mitola in [1] and [2]. From a device perspective, cognitive radios were envisioned by Mitola as intelligent agents that are capable of sensing the environment to identify the locations of possible spectrum holes. The aim is dynamical fitting inside spectrum holes while observing and learning from the parameters obtained from the surrounding wireless scene and while avoiding harmful interference with legacy users. The concept of cognitive radios has received great attention from the research community as it poses as a promising technique that enables exploitation of underutilized spectrum. The IEEE 802.22 standard for wireless regional area networks (WRANs) is the first cognitive radio-based standard [3].

On the other hand, licensed shared access (LSA) is a recently evolving direction that takes advantage of the CR concepts [4]. Within a cognitive radio context, exempted devices are known as secondary users (SUs) whereas original license owners are known as primary users (PUs). However, within the LSA concept, the equivalent of a SU is an *LSA-Licensee* and an *incumbent* for a PU. Thus, the concept of spectrum sensing is crucial to ensure an interference-free mode of operation that will not harm legacy users. Generally, the problem of spectrum sensing or detection of primary users has become increasingly important, and recently the IEEE 802.22 WRAN Spectrum Occupancy Sensing (SOS) Study Group have been launched to develop spectrum sensing standards [5].

A considerable amount of studies investigating various techniques of spectrum sensing have been carried out, such as [6] and [7]. However, not much of the current literature pays particular attention to detection over the frequency dimension using spectrum estimates. In fact, there is a large volume of published studies describing and analyzing time domain (TD) approaches such as the energy detector (ED) in particular and other TD-based eigenvalue techniques (see [8], [9] and references therein). In frequency domain (FD), nonparametric spectrum estimators include the periodogram, Bartlett method, Welch's method of overlapped segmented averaging (WOSA) and the multitaper method (MTM). The multitaper method has other various applications in geophysics and signal and data processing, e.g., radiographic image analysis and radar sea-clutter classification. In [10], Haykin strongly advocated MTM as part of his signal processing vision of the use of cognitive radios for opportunistic spectrum access. It is well known in the literature that the problem of power spectral density (PSD) estimation is challenged by the bias-variance dilemma [11]. However, centered on a specific frequency, the multitaper method mitigates the dilemma as the signal is expanded within a fixed bandwidth. This impact results from the orthonormal properties of special windowing functions, which are known as the discrete prolate spheriodal sequences (DPSSs) [12].

B. Previous Work and Motivations

Detection based on nonparametric PSD estimators was addressed in [13]–[20]. The presented study in [14] considered the periodogram, whereas Bartlett's method was considered in [15], WOSA method was considered in

[16] and finally the multitaper method was considered in [17]–[20]. Focusing on previous work for the multitaper method, [17] considered raw multitapering performed by a single secondary user to detect the presence of a primary user. However, this study considered additive white Gaussian noise (AWGN) only, and then [18] upgraded the model presented in [17] to include non-zero mean signal constellations where the performance was formulated in terms of the Marcum Q-function. Also, [20] addressed the performance of the multitaper method for both cases of accurate and inaccurate noise variance, by using approximations methods for the threshold. However, [20] did not focus on fading and addressed the probability of detection in only two operation environments: deterministic signals in AWGN and a Gaussian signal. Finally, the multitaper method combined with singular value decomposition (SVD) was considered in [19] but without presentation of any accurate or closed form formulas or taking the impact of fading into account. In addition, [19] didn't assume the original decision variable that was proposed by Haykin in [10] neither did the authors in [20]. Hence, in contrast with what was done previously in the literature, we tackle all aforementioned issues by accurate mapping of the multitaper estimate into the Phase-Type class of statistical distributions while assuming propagation over fading channels.

C. Contributions

In this paper, we address two specific scenarios for the multitaper method. First, since multiple-input-multiple-output (MIMO) antenna systems are widely integrated to provide higher data rates and lower probability of errors; we present the generalized case of sensing with the multitaper method when both the transmitting and sensing nodes employ multiple antennas. Throughout the paper we will refer to this method as MIMO-MTM. Second, we consider the multitaper method combined with singular value decomposition, which is known as the MTM-SVD processor. For both considered multitaper scenarios we present an accurate analysis for the performance of the detector over fading channels. Specifically, we

- formulate the decision variables (for both MIMO-MTM and the MTM-SVD processor) as a Phase-Type positive semidefinite Hermitian form,
- and formulate the **exact** eigenvalues that are associated with the Hermitian form, i.e., the nonzero eigenvalues of the product of the covariance matrix and the Hermitian matrix of the quadratic form
- and we present closed forms for the probabilities of false alarm and missed detection where we also bound the probability of missed detection over Nakagami fading.
- Finally, we address the effect of noise uncertainty at a specific node, and we present accurate expressions for the ergodic probabilities of false alarm and detection.

More specifically, we also derive the optimized detector based on the Neyman-Pearson Approach (NPA) over Nakagami channels. For the case of the MTM-SVD processor, we also assume a case of independent but not identically distributed (i.n.i.d.) fading channels, where the sensing nodes are distributed within a circle centered on the transmitting node.

This article has been accepted for publication in a future issue of this journal, but has not been fully edited. Content may change prior to final publication. Citation information: DOI 10.1109/TSP.2015.2455520, IEEE Transactions on Signal Processing

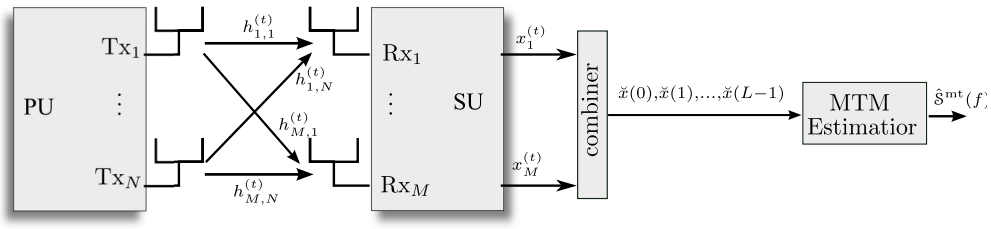

Fig. 1. Structure for MIMO Sensing with Combining and Multitaper Estimation.

D. Paper Organization

The rest of the paper is organized as follows. Section II presents a description of the system model and a preliminary background about the method of multitaper estimation. Section III provides the performance of MIMO-MTM. Section IV considers the multitaper method combined with singular value decomposition for multiple band detection. The effect of noise uncertainty is addressed in Section V. Section VI presents simulation results and finally Section VII provides concluding remarks.

II. Background and System Setup

In this section preliminary information is provided, with a focus on background of the multitaper method of estimation. We explain the basic system model that can be used to obtain a single multitaper estimate within a single-input-single-output (SISO) context, i.e., both the transmitter and the receiving node have single antennas. This system model will be modified throughout the paper to match the addressed detection scenario[1].

A. Mathematical Operators

Following the general trend, throughout this paper vectors will be denoted by lowercase boldface characters and matrices will be denoted by uppercase boldfaced characters. Other mathematical operators that will be used are defined as follows:

- $\log$ is the natural logarithm, and $\log_{10}$ is the common logarithm (Base 10),
- $j = \sqrt{-1}$ is the imaginary unit,
- $(\cdot)^{\mathrm{T}}$ is the transpose,
- $\mathrm{spec}[\cdot]$ is the matrix spectrum,
- $(\cdot)^{\mathrm{H}}$ denotes Hermitian transposition,
- $\langle ., . \rangle$ denotes the inner product,
- $\| \cdot \|_{\mathrm{F}}$ is the Frobenius norm and the subscript is omitted for vectors,

[1]This system model will be modified and explained for each of the considered case of sensing of single-user MIMO primary node with antenna diversity, and the case of the MTM-SVD processor

- $\oplus$ is the direct sum operator,
- $\otimes$ is the Kronecker product,
- $\odot$ denotes the Hadamard product,
- $(\dot{\cdot})$ denotes an estimated parameter,
- $\mathrm{tr}[\cdot]$ is the trace operator,
- $\mathrm{rank}[\cdot]$ is the rank operator,
- $\mathrm{diag}(a_1, \ldots, a_N)$ is a diagonal matrix with elements $a_1, \ldots, a_N$,
- $\mathbb{E}[\cdot]$ represents the statistical expectation operator.

The notations for special matrices are as follows. The identity matrix of size n is $\mathbf{I}_n$, and similarly $\mathbf{O}_n$ is the null matrix, $\mathbf{1}_n$ is the ones vector and $\mathbf{0}_n$ is the null vector.

As far as the concern of spectrum sensing, the null hypothesis $\mathcal{H}_0$ implies that the channel is empty, and the hypothesis $\mathcal{H}_1$ implies that the channel is occupied. The probability of false alarm $\mathcal{P}_{\mathrm{fa}}$, the probability of detection $\mathcal{P}_{\mathrm{d}}$ and the probability of missed detection $\mathcal{P}_{\mathrm{md}}$ are defined as

$$\mathcal{P}_{\mathrm{fa}}(\eta) \triangleq \mathrm{Prob}\left\{D > \eta | \mathcal{H}_0\right\}, \tag{1a}$$

$$\mathcal{P}_{\mathrm{d}}(\eta) \triangleq \mathrm{Prob}\left\{D > \eta | \mathcal{H}_1\right\}, \tag{1b}$$

$$\mathcal{P}_{\mathrm{md}}(\eta) \triangleq \mathrm{Prob}\left\{D \leq \eta | \mathcal{H}_1\right\}, \tag{1c}$$

where η is a chosen sensing threshold and D is the decision variable.

B. Multitaper Estimation

Let $x^{(t)}$ denote the instantaneously observed signal by the sensing node within a time frame of length L, i.e, $t = 0, \ldots, L-1$, and let $\hat{\mathcal{S}}^{\mathrm{mt}}(f)$ denote the multitaper estimate at the f-th frequency (index).

1) The Slepian Sequences: The idea of multitaper estimation depends on using a set of orthonormal sequences known as the *Discrete Prolate Spheriodal Sequences* (DPSS), and also known as the Slepian Sequences [21]. Hence, before computation of the multitaper estimate, a number of K Slepain tapers should be prepared. Let $\boldsymbol{\nu}^{(k)}(L, W) = \{\nu_t^{(k)}(L, W)\}_{t=1}^{L}$ denote the k-th order Slepian taper, where $k = 0, 1, \ldots, K-1$ and let λ_k denotes the corresponding k-th energy concentration. It is assumed that the Slepian sequences are ordered in descending order based on their energy concentrations. Centered on f, the Slepian sequences have the maximal energy concentration within the bandwidth $(f - W,\ f + W)$. This allows the legendary problem of the bias-variance dilemma to be replaced by a bias-resolution trade-off. Furthermore, the total number of the orthonormal tapers is limited by the $K \leq \lfloor 2LW \rfloor$, which defines the degrees of freedom (DoF) for adjusting the variance of the estimate. Also, the concentrations start to approach zero for values beyond $2LW - 1$. Note that the common choices for half the time-bandwidth product are 2.5, 3, 3.5, and 4. However, other ranges for the time-bandwidth product are from 6 to 10, while the number of Slepian sequences extends from 10 up to 16 [22], [23].

2) Alternative Formulation for The Multitaper Method: Usually the spectrum estimate is computed from the first eigenspectra that demonstrate the minimal sidelobe leakage. Because of this issue some software packages give the option of dropping the last order taper(s). Using the weights $a_0, a_1, \ldots, a_{K-1}$, where $a_i \in \mathbb{R}^+$, the conventional expression to obtain the multitaper estimate from the discrete time observations $\{x^{(t)}\}_{t=0}^{L-1}$ is [11]

$$\hat{\mathcal{S}}^{\mathrm{mt}}(f) = \frac{\sum_{k=0}^{K-1} a_k(f) \left| \sum_{t=0}^{L-1} \nu_t^{(k)}(L,W) x^{(t)} e^{-j2\pi f t} \right|^2}{\sum_{i=0}^{K-1} a_i(f)}. \tag{2}$$

There are three options for choosing a value for the weighting elements $a_0, a_1, \ldots, a_{K-1}$ which are: unity weights, the energy concentrations associated with the employed Slepian sequences and the last option is using adaptive weights. The representation of the multitaper estimate given by (2) is a conventional representation. However, the estimator $\hat{\mathcal{S}}^{\mathrm{mt}}(f)$ can be written as the positive semidefinite Hermitian form that is given by

$$\hat{\mathcal{S}}^{\mathrm{mt}}(f) = \frac{\sum_{k=0}^{K-1} a_k(f)\, \mathbf{x}^{\mathrm{H}} {\boldsymbol{\Psi}^{(k)}}^{\mathrm{T}}{}_{(L,W)}\, \boldsymbol{\Phi}(f)\, \boldsymbol{\Psi}^{(k)}{}_{(L,W)} \mathbf{x}}{\sum_{i=0}^{K-1} a_i(f)}, \tag{3}$$

where $\mathbf{x} = \begin{bmatrix} x^{(0)} & \ldots & x^{(L-1)} \end{bmatrix}^{\mathrm{T}}$ and $\boldsymbol{\Psi}^{(k)} \in \mathbb{R}^{L \times L}$ is given by

$$\boldsymbol{\Psi}^{(k)}{}_{(L,W)} = \mathrm{diag}\left(\nu_0^{(k)}{}_{(L,W)}, \ldots, \nu_{L-1}^{(k)}{}_{(L,W)} \right), \quad 0 \le k \le K-1, \tag{4}$$

and $\boldsymbol{\Phi}(f) \in \mathbb{C}^{L \times L}$ is given by

$$\boldsymbol{\Phi}(f) = \boldsymbol{\xi}(f)^{\mathrm{H}} \boldsymbol{\xi}(f), \tag{5}$$

where

$$\boldsymbol{\xi}(f) = \begin{bmatrix} 1 & \xi_f & \xi_f^2 & \ldots & \xi_f^{L-1} \end{bmatrix}, \tag{6}$$

and ξ_f is the primitive L-th root of unity for the f-th frequency index. Hence, the matrix that results from the product ${\boldsymbol{\Psi}^{(k)}}^{\mathrm{H}} \boldsymbol{\Phi}(f) \boldsymbol{\Psi}^{(k)}$ can be written as:

$$\begin{aligned} &{\boldsymbol{\Psi}^{(k)}}^{\mathrm{T}}{}_{(L,W)}\, \boldsymbol{\Phi}(f)\, \boldsymbol{\Psi}^{(k)}{}_{(L,W)} \\ &\quad = \begin{bmatrix} {\nu_0^{(k)}}^2{}_{(L,W)} & \nu_1^{(k)}{}_{(L,W)} \nu_0^{(k)}{}_{(L,W)} \xi_f^{-1} & \ldots & \nu_0^{(k)}{}_{(L,W)} \nu_{L-1}^{(k)}{}_{(L,W)} \xi_f^{L-1} \\ \nu_1^{(k)}{}_{(L,W)} \nu_0^{(k)}{}_{(L,W)} \xi_f & {\nu_1^{(k)}}^2{}_{(L,W)} & \ldots & \nu_1^{(k)}{}_{(L,W)} \nu_{L-1}^{(k)}{}_{(L,W)} \xi_f^{L-2} \\ \vdots & \vdots & \ddots & \vdots \\ \nu_0^{(k)}{}_{(L,W)} \nu_{L-1}^{(k)}{}_{(L,W)} \xi_f^{L-1} & \nu_1^{(k)}{}_{(L,W)} \nu_{L-1}^{(k)}{}_{(L,W)} \xi_f^{L-2} & \ldots & {\nu_{L-1}^{(k)}}^2{}_{(L,W)} \end{bmatrix}. \end{aligned} \tag{7}$$

Looking into the previous equation, it can be seen that the following properties hold true:

$$\mathrm{rank}\left[{\boldsymbol{\Psi}^{(k)}}^{\mathrm{T}}{}_{(L,W)}\, \boldsymbol{\Phi}(f)\, \boldsymbol{\Psi}^{(k)}{}_{(L,W)} \right] = 1, \tag{8a}$$

$$\mathrm{tr}\left[{\boldsymbol{\Psi}^{(k)}}^{\mathrm{T}}{}_{(L,W)} \boldsymbol{\Phi}(f) \boldsymbol{\Psi}^{(k)}{}_{(L,W)} \right] = \left\{ \sum_{i=0}^{L-1} {\nu_i^{(k)}}^2{}_{(L,W)} \right\}. \tag{8b}$$

This article has been accepted for publication in a future issue of this journal, but has not been fully edited. Content may change prior to final publication. Citation information: DOI 10.1109/TSP.2015.2455520, IEEE Transactions on Signal Processing

III. Exact Analysis of the Multitaper Detector Assuming MIMO Structure with Data Combining

A. System Model

Let us consider a primary user network, in which each user is equipped with a number of N transmit antennas. At the receiving side, the secondary system is equipped with a number of M antennas where $M \geq N$ as illustrated in Fig.1. For each hypothesis, the overall received signal at the t-th time instant is given by

$$\mathbf{x}(t) = \begin{cases} \mathbf{n}(t), & \mathcal{H}_0, \\ \mathbf{H}(t)\mathbf{s}(t) + \mathbf{n}(t), & \mathcal{H}_1, \end{cases} \tag{9}$$

where $\mathbf{x}(t) \in \mathbb{C}^{M\times 1}$ is the received signal vector, $\mathbf{H}(t) \in \mathbb{C}^{M\times N}$ is the channel matrix, $\mathbf{s}(t) \in \mathbb{C}^{N\times 1}$ is the transmitted symbols vector and $\mathbf{n}(t) \in \mathbb{C}^{M\times 1}$ denotes the noise vector. Let us also define

$$\mathbf{x}(t) \triangleq \begin{bmatrix} x_1^{(t)} & \dots & x_M^{(t)} \end{bmatrix}^{\mathrm{T}}, \tag{10a}$$

$$\mathbf{s}(t) \triangleq \begin{bmatrix} s_1^{(t)} & \dots & s_N^{(t)} \end{bmatrix}^{\mathrm{T}}, \tag{10b}$$

$$\mathbf{n}(t) \triangleq \begin{bmatrix} n_1^{(t)} & \dots & n_M^{(t)} \end{bmatrix}^{\mathrm{T}}, \tag{10c}$$

where $s_i^{(t)}$ is the transmitted signal from the i-th antenna, which is assumed zero mean with the constraint $\mathbb{E}[\mathbf{s}^{\mathrm{H}}\mathbf{s}] \leq \sigma_s^2$. The transmitted signals $\{s_i^{(t)}\}_{i=1}^N$ are independent zero-mean circular symmetric complex Gaussian variables with variance σ^2/N. The instantaneous noise $n_i^{(t)}$ is a circular symmetric additive white Gaussian noise process with variance $\mathbb{E}[|n_i^{(t)}|^2] = \sigma_n^2$, and we also assume that the noise process is spatially white. The channel matrix $\mathbf{H}(t)$ is assumed spatially rich, with independent and identically distributed (i.i.d.) elements, and has the form

$$\mathbf{H}(t) = \begin{bmatrix} h_{1,1}^{(t)} & \dots & h_{1,N}^{(t)} \\ \vdots & \ddots & \vdots \\ h_{M,1}^{(t)} & \dots & h_{M,N}^{(t)} \end{bmatrix}, \tag{11}$$

where $h_{m,i}^{(t)}$ is the instantaneous channel from the i-th transmit antenna to the m-th receiver. Henceforth, at the receiving side the signal received by the i-th branch at the t-th time instant is

$$x_i^{(t)} = \begin{cases} n_i^{(t)}, & \mathcal{H}_0, \\ \sum_{p=1}^N h_{i,p}^{(t)} s_p^{(t)} + n_i^{(t),} & \mathcal{H}_1, \end{cases} \tag{12}$$

where $t = 0, \dots, L-1$ and $i = 1, \dots, M$.

This article has been accepted for publication in a future issue of this journal, but has not been fully edited. Content may change prior to final publication. Citation information: DOI 10.1109/TSP.2015.2455520, IEEE Transactions on Signal Processing

B. Combining Followed by Multitaper Estimation

Let $\breve{\mathbf{x}} = \{\breve{x}(t)\}_{t=0}^{L-1}$ be the column vector consisting of the instantaneous equally combined[2] output signal, i.e., $\breve{x}(t) = \sum_{i=1}^{M} x_i^{(t)}$, where for the case of $\mathcal{H}_0$ we have $\breve{x}(t) \sim \mathcal{CN}\left(0, M\sigma_n^2\right)$, and for the case of $\mathcal{H}_1$ we have $\breve{x}(t) \sim \mathcal{CN}\left(0, \frac{\sigma_s^2}{N}\sum_{p=1}^{N}\left|\sum_{i=1}^{M} h_{i,p}^{(t)}\right|^2 + M\sigma_n^2\right)$. Conditioned on the channel gains, by the end of the sensing frame of L samples, we have

$$\mathcal{H}_0: \quad \breve{\mathbf{x}} \sim \mathcal{CN}\left(\mathbf{0}_L, \sigma_n^2 M \mathbf{I}_L\right), \tag{13a}$$

$$\mathcal{H}_1: \quad \breve{\mathbf{x}} \sim \mathcal{CN}\left(\mathbf{0}_L, \sigma_s^2 \breve{\mathbf{H}}\breve{\mathbf{H}}^{\mathrm{H}} + \sigma_n^2 M \mathbf{I}_L\right), \tag{13b}$$

where

$$\breve{\mathbf{H}}\breve{\mathbf{H}}^{\mathrm{H}} \equiv \frac{1}{N}\mathrm{diag}\left(\sum_{p=1}^{N}\left|\sum_{i=1}^{M} h_{i,p}^{(0)}\right|^2, \sum_{p=1}^{N}\left|\sum_{i=1}^{M} h_{i,p}^{(1)}\right|^2, \ldots, \sum_{p=1}^{N}\left|\sum_{i=1}^{M} h_{i,p}^{(L-1)}\right|^2\right). \tag{14}$$

The multitaper estimate can be written as the Hermitian form that is given by

$$\hat{\mathbb{S}}^{\mathrm{mt}}(f) = \frac{a_k(f)}{\sum_{i=0}^{K-1} a_i(f)} \mathrm{vec}\left(\breve{\mathbf{x}} \otimes \mathbf{1}_K^{\mathrm{T}}\right)^{\mathrm{H}} \bigoplus_{k=0}^{K-1} {\boldsymbol{\Psi}^{(k)}}^{\mathrm{T}}{}_{(L,W)}\, \boldsymbol{\Phi}(f)\, \boldsymbol{\Psi}^{(k)}{}_{(L,W)}\, \mathrm{vec}\left(\breve{\mathbf{x}} \otimes \mathbf{1}_K^{\mathrm{T}}\right). \tag{15}$$

Generally, in order to obtain the statistical distributions of a given Hermitian form, it is required to derive expressions for the eigenvalues associated with the Hermitian form under scrutiny [24]. Looking into the Hermitian form given by (15), the Hermitian matrix of the Hermitain form is

$$\frac{a_k(f)}{\sum_{i=0}^{K-1} a_i(f)} \bigoplus_{k=0}^{K-1} {\boldsymbol{\Psi}^{(k)}}^{\mathrm{T}}{}_{(L,W)}\, \boldsymbol{\Phi}(f)\, \boldsymbol{\Psi}^{(k)}{}_{(L,W)}.$$

Thus, in this case the eigenvalues of the Hermtian form in (15) are the eigenvalues of the matrix that results from the product of the covariance matrix of $\mathrm{vec}\left(\breve{\mathbf{x}} \otimes \mathbf{1}_K^{\mathrm{T}}\right)^{\mathrm{H}}$ and the Hermitian matrix associated with the Hermitian form.

Theorem *1 (Eigenvalues of the Hermitian form given by* (15)*):* The positive semi-definite Hermitian form given by (15) has LK eigenvalues, but with only K nonzero eigenvalues. Assuming the case of the null hypothesis $\mathcal{H}_0$, the k-th nonzero eigenvalue is given by

$$\ell_0^{(k)} = \frac{a_k}{\sum_{i=0}^{K-1} a_i} M\sigma_n^2 \|\boldsymbol{\nu}^{(k)}\|^2, \tag{16}$$

and assuming the case of the alternate hypothesis $\mathcal{H}_1$, the k-th nonzero eigenvalue is given by

$$\ell_1^{(k)} = \frac{a_k}{\sum_{i=0}^{K-1} a_i}\left(\frac{1}{N}\sigma_s^2 \sum_{t=1}^{L}\sum_{p=1}^{N}\left|\sum_{i=1}^{M} h_{i,p}^{(t)}\right|^2 {\nu_t^{(k)}}^2 + M\sigma_n^2\|\boldsymbol{\nu}^{(k)}\|^2\right). \tag{17}$$

[2]The use of MIMO here aids in faster collection of signals, and mitigates the impact of noise. Equal combining is employed since the channel from the primary transmitting node to the secondary sensing node is assumed to be unknown. Other combining techniques that requires channel state informations (CSI), such as maximal ratio combining (MRC) are used only within the context of cooperative spectrum sensing in the reporting channels.

This article has been accepted for publication in a future issue of this journal, but has not been fully edited. Content may change prior to final publication. Citation information: DOI 10.1109/TSP.2015.2455520, IEEE Transactions on Signal Processing

Proof: Let $\boldsymbol{\Sigma}_{\breve{\mathbf{x}}}$ be the covariance matrix of $\breve{\mathbf{x}}$ and let $\boldsymbol{\Sigma}_{\breve{\mathbf{x}},\mathrm{EGC}}$ be the covariance matrix that is associated with the Hermitian form in (15). We have

$$\boldsymbol{\Sigma}_{\breve{\mathbf{x}}} \triangleq \mathbb{E}\left[\breve{\mathbf{x}}\breve{\mathbf{x}}^{\mathrm{H}}\right], \tag{18}$$

$$\boldsymbol{\Sigma}_{\breve{\mathbf{x}},\mathrm{EGC}} \triangleq \mathbb{E}\left[\mathrm{vec}\left(\breve{\mathbf{x}} \otimes \mathbf{1}_K^{\mathrm{T}}\right) \mathrm{vec}\left(\breve{\mathbf{x}} \otimes \mathbf{1}_K^{\mathrm{T}}\right)^{\mathrm{H}}\right]. \tag{19}$$

Since $\mathrm{rank}[\boldsymbol{\Sigma}_{\breve{\mathbf{x}},\mathrm{EGC}}] = LK$ and $\mathrm{rank}[\boldsymbol{\Phi}_f] = 1$ then it follows that

$$\mathrm{rank}\left[\bigoplus_{k=0}^{K-1} \boldsymbol{\Phi}(f)\right] = \mathrm{rank}\left[\bigoplus_{k=0}^{K-1} {\boldsymbol{\Psi}^{(k)}}^2{}_{(L,W)} \bigoplus_{k=0}^{K-1} \boldsymbol{\Phi}(f)\right], \tag{20}$$

and then we can conclude that

$$\begin{aligned} &\mathrm{rank}\left[\boldsymbol{\Sigma}_{\breve{\mathbf{x}},\mathrm{EGC}} \bigoplus_{k=0}^{K-1} {\boldsymbol{\Psi}^{(k)}}^{\mathrm{T}}{}_{(L,W)}\, \boldsymbol{\Phi}(f)\, \boldsymbol{\Psi}^{(k)}{}_{(L,W)}\right], \\ &\quad = \mathrm{rank}\left[\bigoplus_{k=0}^{K-1} \boldsymbol{\Phi}(f)\right] \\ &\quad = K. \end{aligned} \tag{21}$$

Next, to find the exact value of the eigenvalue under each hypothesis, each nonzero eigenvalue corresponds to the part of the spectrum estimate that is computed from the k-th Slepian sequence. Therefore, the k-th eigenvalue is $\mathrm{tr}[\boldsymbol{\Sigma}_{\breve{\mathbf{x}}} {\boldsymbol{\Psi}^{(k)}}^{\mathrm{T}}{}_{(L,W)} \boldsymbol{\Phi}(f) \boldsymbol{\Psi}^{(k)}{}_{(L,W)}]$ and assuming $\mathcal{H}_0$ we get the expression given by (16), and assuming the alternate hypothesis $\mathcal{H}_1$ we arrive at the expression given by (17). ■

C. Estimation with Generalized/Distinct Weights

With the aid of [25, Ch.10], a Hermitian quadratic form with *distinct* eigenvalues has a PDF which is a weighted sum of exponential kernels. In this case, the weights reported in [25] can be seen as scaled values of the Lagrange basis polynomials that are associated with the nonzero eigenvalues of the Hermitian quadratic form. This case is a hypoexponential[3] variable with distinct parameters. However, the performance for generic values can be obtained, which will be explained as follows. By making use of the results from Theorem 1, and summing the K weighted eigenspectra the total spectrum estimate is a Phase-Type distributed variable, where a generalized PDF is given by

$$f(x; \boldsymbol{\alpha}, \mathfrak{Z}) = -\boldsymbol{\alpha}_K^{\mathrm{T}} \exp\left(x\mathfrak{Z}\right) \mathfrak{Z}\mathbf{1}_K, \quad x \geq 0, \tag{22}$$

where $\boldsymbol{\alpha} = [1, 0, \ldots, 0]$ is a $K \times 1$ probability vector and $\mathfrak{Z} \in \mathbb{R}^{K \times K}$ is the subgenerator matrix, which employs a form that is subject to the considered hypothesis. For further understanding of the generic structure of subgenerator matrices, the reader is referred to [28] and [29]. Assuming the case of the hypothesis $\mathcal{H}_0$, the probability of false alarm is

$$\mathcal{P}_{\mathrm{fa}}(\eta; \boldsymbol{\alpha}, \mathfrak{Z}_0) = \int_{\eta}^{\infty} f(x; \boldsymbol{\alpha}, \mathfrak{Z}_{\mathbf{0}})\, \mathrm{d}x = \boldsymbol{\alpha}_K^{\mathrm{T}} \exp\left(\eta\mathfrak{Z}_0\right) \mathbf{1}_K, \tag{23}$$

[3]The hypoexponential distribution [26], [27] generalizes the Erlang distribution. It can be viewed as a special case of the Phase-Type distribution as it represents a mixture of phases that can be identical or non-identical.

This article has been accepted for publication in a future issue of this journal, but has not been fully edited. Content may change prior to final publication. Citation information: DOI 10.1109/TSP.2015.2455520, IEEE Transactions on Signal Processing

where $\mathfrak{Z}_0$ ia a function of the nonzero eigenvalues $\ell_0^{(0)},\ldots,\ell^{(K-1)}$ obtained in Theorem 1, and is defined as

$$\mathfrak{Z}_0 = \frac{\sum_{k=0}^{K-1} a_k}{M\sigma_n^2}\begin{bmatrix} -a_0^{-1} & a_0^{-1} & 0 & \ldots & 0 \\ 0 & -a_1^{-1} & a_1^{-1} & \ldots & 0 \\ 0 & 0 & -a_2^{-1} & \ddots & 0 \\ \vdots & \vdots & \vdots & \ddots & \vdots \\ 0 & 0 & 0 & \ldots & -a_{K-1}^{-1} \end{bmatrix}. \tag{24}$$

The previous result given by (23) can be used for any value of the weights $a_1,\ldots,a_{K-1}$. However, for the case of distinct weights, the probability of false alarm can be written as

$$\mathcal{P}_{\rm fa}(\eta) = \sum_{i=0}^{K-1} \exp\left(-\frac{\eta}{a_i M\sigma_n^2 \left\|\boldsymbol{\nu}^{(i)}(L,W)\right\|^2}\sum_{k=0}^{K-1} a_k\right) \prod_{\substack{q=0\\ q\neq i}}^{K-1} \frac{a_i \left\|\boldsymbol{\nu}^{(i)}(L,W)\right\|^2}{a_i \left\|\boldsymbol{\nu}^{(i)}(L,W)\right\|^2 - a_q \left\|\boldsymbol{\nu}^{(q)}(L,W)\right\|^2}. \tag{25}$$

On the other hand, assuming the alternate hypothesis $\mathcal{H}_1$, let us define $\boldsymbol{\vartheta}$ and $\boldsymbol{\nu}_2^{(k)}$ as

$$\boldsymbol{\vartheta} = \begin{bmatrix} \vartheta_0 & \ldots & \vartheta_{L-1} \end{bmatrix}^{\rm T}, \tag{26a}$$

$$\vartheta_t = \sum_{n=1}^{N}\left|\sum_{m=1}^{M} h_{m,n}^{(t)}\right|^2, \tag{26b}$$

$$\boldsymbol{\nu}_2^{(k)} = \boldsymbol{\nu}^{(k)} \odot \boldsymbol{\nu}^{(k)}. \tag{26c}$$

Thus, the probability of missed detection is obtained as

$$\begin{aligned} \mathcal{P}_{\rm md}(\eta;\boldsymbol{\alpha},\mathfrak{Z}_1) &= 1 - \int_{\eta}^{\infty} f(x;\boldsymbol{\alpha},\mathfrak{Z}_{\mathbf{1}})\,{\rm d}x \\ &= 1 - \boldsymbol{\alpha}_K^{\rm T} \exp\left(\eta\mathfrak{Z}_1\right)\mathbf{1}_K. \end{aligned} \tag{27}$$

By making use of the results from Theorem 1, $\mathfrak{Z}_1$ have the form given by

$$\mathfrak{Z}_1 = N\sum_{k=0}^{K-1} a_k \times \begin{bmatrix} \frac{-a_0^{-1}}{\sigma_s^2\langle\boldsymbol{\vartheta},\boldsymbol{\nu}_2^{(0)}\rangle + NM\sigma_n^2\|\boldsymbol{\nu}_{\mathbf{2}}{}^{(0)}\|^2} & \frac{a_0^{-1}}{\sigma_s^2\langle\boldsymbol{\vartheta},\boldsymbol{\nu}_2^{(0)}\rangle + NM\sigma_n^2\|\boldsymbol{\nu}_{\mathbf{2}}{}^{(0)}\|^2} & 0 & \ldots & 0 \\ 0 & \frac{-a_1^{-1}}{\sigma_s^2\langle\boldsymbol{\vartheta},\boldsymbol{\nu}_2^{(1)}\rangle + NM\sigma_n^2\|\boldsymbol{\nu}_{\mathbf{2}}{}^{(1)}\|^2} & \frac{a_1^{-1}}{\sigma_s^2\langle\boldsymbol{\vartheta},\boldsymbol{\nu}_2^{(1)}\rangle + NM\sigma_n^2\|\boldsymbol{\nu}_{\mathbf{2}}{}^{(1)}\|^2} & \ldots & 0 \\ 0 & 0 & \frac{-a_2^{-1}}{\sigma_s^2\langle\boldsymbol{\vartheta},\boldsymbol{\nu}_2^{(2)}\rangle + NM\sigma_n^2\|\boldsymbol{\nu}_{\mathbf{2}}{}^{(2)}\|^2} & \ddots & 0 \\ \vdots & \vdots & \vdots & \ddots & \vdots \\ 0 & 0 & 0 & \ldots & \frac{-a_{K-1}^{-1}}{\sigma_s^2\langle\boldsymbol{\vartheta},\boldsymbol{\nu}_2^{(K-1)}\rangle + NM\sigma_n^2\|\boldsymbol{\nu}_{\mathbf{2}}{}^{(K-1)}\|^2} \end{bmatrix}. \tag{28}$$

Similarly, for distinct eigenvalues the probability of missed detection can be written as given by

$$\mathcal{P}_{\rm md}(\eta) = 1 - \sum_{i=0}^{K-1}\exp\left(\frac{-\eta a_i^{-1}\sum_{k=0}^{K-1} a_k}{M\sigma_n^2\|\boldsymbol{\nu}^{(i)}(L,W)\|^2 + \frac{1}{N}\sigma_s^2\sum_{t=1}^{L}\sum_{n=1}^{N}\left|\sum_{m=1}^{M} h_{m,n}^{(t)}\right|^2 {\nu_t^{(i)}}^2(L,W)}\right)$$

$$\times \prod_{\substack{q=0\\ q\neq i}}^{K-1} \frac{a_i\sigma_s^2\sum_{t=1}^{L}\sum_{n=1}^{N}\left|\sum_{m=1}^{M} h_{m,n}^{(t)}\right|^2 {\nu_t^{(i)}}^2(L,W) + a_i NM\sigma_n^2\|\boldsymbol{\nu}^{(i)}(L,W)\|^2}{\sigma_s^2\sum_{t=1}^{L}\sum_{n=1}^{N}\left|\sum_{m=1}^{M} h_{m,n}^{(t)}\right|^2 \left(a_i{\nu_t^{(i)}}^2(L,W) - a_q{\nu_t^{(q)}}^2(L,W)\right) + NM\sigma_n^2\left(a_q\|\boldsymbol{\nu}^{(q)}(L,W)\|^2 - a_i\|\boldsymbol{\nu}^{(i)}(L,W)\|^2\right)}. \tag{29}$$

This article has been accepted for publication in a future issue of this journal, but has not been fully edited. Content may change prior to final publication. Citation information: DOI 10.1109/TSP.2015.2455520, IEEE Transactions on Signal Processing

In fact, when using the energy concentrations of the Slepian sequences as weights, some of the weights of the exponential kernels in (25) and (29) may approach infinity when the denominator approaches zero, since the energy concentrations will be very close or equal to 1. In this case, the generalized forms given by (23) and (27) should be used.

D. Estimation with Unity Weights

Based on the previous results, let us consider the case of applying unity weights to (15), i.e., $a_0, \ldots, a_{K-1} = 1$. Assuming the null hypothesis, and since $\|\boldsymbol{\nu}^{(k)}{}_{(L,W)}\|^2 \approx 1$ the probability of false alarm is given by

$$\mathcal{P}_{\mathrm{fa}}(\eta) = \frac{1}{\Gamma(K)}\Gamma\left(K, \frac{K\eta}{\sigma_n^2 M}\right). \tag{30}$$

where $\Gamma(\cdot)$ denotes the gamma function and $\Gamma(.,.)$ is the upper incomplete gamma function as defined in [30]. Similarly the probability of missed detection is given by

$$\mathcal{P}_{\mathrm{md}}(\eta) = 1 - \sum_{i=0}^{K-1} \exp\left(\frac{-\eta N K}{N M \sigma_n^2 + \sigma_s^2 \left\langle \boldsymbol{\vartheta}, \boldsymbol{\nu}_2^{(i)}{}_{(L,W)} \right\rangle}\right) \prod_{q=0, q\neq i}^{K-1} \frac{N M \sigma_n^2 + \sigma_s^2 \left\langle \boldsymbol{\vartheta}, \boldsymbol{\nu}_2^{(i)}{}_{(L,W)} \right\rangle}{\sigma_s^2 \left\langle \boldsymbol{\vartheta}, \boldsymbol{\nu}_2^{(i)}{}_{(L,W)} - \boldsymbol{\nu}_2^{(q)}{}_{(L,W)} \right\rangle}. \tag{31}$$

E. Optimal Ergodic Performance over Nakagami Fading Channels

1) Maximum Average Probability of Miss: Let us assume that the instantaneous channel envelope from the n-th transmit antenna to the m-th receive antenna is an $\mathfrak{m}$-Nakagami process with shape parameter $\mathfrak{m}$ and spread parameter Ω. Moreover, let $\gamma_m^{(t)}$ be the instantaneous signal-to-noise-ratio (SNR) for the m-th branch, where $t = 0, \ldots, L-1$ and $m = 1, \ldots, M$. Let us also assume that $\mathbb{E}[\gamma_1^{(t)}] = \cdots = \mathbb{E}[\gamma_M^{(t)}] = \overline{\gamma}$. Looking into (29), since $\vartheta_t \sim \mathrm{Gamma}(N, M\Omega)$, then $\sum_{t=0}^{L-1}\sum_{m=1}^{M} \gamma_m^{(t)} \nu_t^{(k)}$ is a mixture of the instantaneous SNR weighted with instantaneous values of the k-th Slepian vector. This is a case of a hypoexponential variable with NL rate parameters, which is equivalent to a Phase-Type distribution with a $1 \times NL$ probability vector and an $NL \times NL$ subgenerator matrix. In this case, since

$$\mathbb{E}\left[\sum_{t=0}^{L-1}\sum_{m=1}^{M} \gamma_m^{(t)} {\nu_t^{(k)}}^2{}_{(L,W)}\right] = \overline{\gamma} M \|\boldsymbol{\Psi}^{(k)}{}_{(L,W)}\|_{\mathrm{F}}^2, \tag{32}$$

then applying Jensen's inequality gives the minimum bound for the average probability of missed detection as $\mathbb{E}[\mathcal{P}_{\mathrm{md}}(\eta, \gamma)] \geq \mathcal{P}_{\mathrm{md}}(\eta, \mathbb{E}[\gamma])]$. Assuming distinct weights $a_0, \ldots, a_{K-1}$ the minimum average probability of missed detection is

$$\overline{\mathcal{P}}_{\mathrm{md}}(\eta) \leq 1 - \sum_{i=0}^{K-1} \exp\left(\frac{-\eta \sum_{k=0}^{K-1} a_k}{a_i \sigma_n^2 M (\overline{\gamma}+1)}\right) \prod_{\substack{q=0,\\ q\neq i}}^{K-1} \frac{a_i}{(a_i - a_q)} \tag{33}$$

and when all weights are unity the Phase-Type distribution of the mixture $\sum_{t=0}^{L-1}\sum_{m=1}^{M} \gamma_m^{(t)} \nu_t^{(k)}$ is reduced into the Erlang distribution, and hence the average minimum probability of missed detection is

$$\mathcal{P}_{\mathrm{md,min}}(\eta, \overline{\gamma}) = \frac{1}{\Gamma(K+1)} \exp\left(\frac{-\eta K}{\overline{\gamma}+1}\right) \left(\frac{\eta K}{\overline{\gamma}+1}\right)^K {}_1F_1\left(1; K+1; \frac{\eta K}{\overline{\gamma}+1}\right). \tag{34}$$

where ${}_1F_1(\cdot;\cdot;\cdot)$ is Kummer's confluent hypergeometric function.

This article has been accepted for publication in a future issue of this journal, but has not been fully edited. Content may change prior to final publication. Citation information: DOI 10.1109/TSP.2015.2455520, IEEE Transactions on Signal Processing

2) Optimal Probability of Detection: Let δ denote a predefined probability of false alarm. Hence the likelihood ratio is given by $\frac{p(z;\mathcal{H}_1)}{p(z;\mathcal{H}_0)}$ where $p(z;\mathcal{H}_0) \triangleq -\frac{\partial}{\partial z}\mathcal{P}_{\rm fa}(z)$ and $p(z;\mathcal{H}_0) \triangleq \frac{\partial}{\partial z}\mathcal{P}_{\rm md}(z)$, and hence the test will have the form

$$(\overline{\gamma}+1)^{-K}\exp\left(\frac{z\overline{\gamma}K}{\sigma_n^2 M(\overline{\gamma}+1)}\right)\underset{\mathcal{H}_0}{\overset{\mathcal{H}_1}{\gtrless}}\eta(\delta), \tag{35}$$

where $\eta(\delta)$ is the sensing threshold that yields the predefined probability of false alarm δ. Hence, the test can be rewritten in the form

$$z \geq \log\left(\eta(\overline{\gamma}+1)^K\right)\frac{\sigma_n^2 M(\overline{\gamma}+1)}{\overline{\gamma}K}. \tag{36}$$

The threshold is chosen to satisfy the constraint $\int_\eta^\infty p(z;\mathcal{H}_0)\,\mathrm{d}z = \delta$, [31], [32]. The modified threshold is

$$\eta'(\delta) = \left(\eta(\overline{\gamma}+1)^K\right)\frac{\sigma_n^2 M(\overline{\gamma}+1)}{\overline{\gamma}K}. \tag{37}$$

The probability of false alarm in (30) can be inverted by making use of the function $Q^{-1}(\cdot,\cdot)$, which is the inverse regularized incomplete (upper) gamma function [33].

IV. Exact Analysis using the MTM-SVD Processor

The MTM-SVD processor is a collaborative variation of the multitaper detector in which a number of users cooperate by sending their local eigenspectra to be processed by a central node. In this part, the performance of the MTM-SVD processor is investigated over fading channels.

A. System Model

In this section, let us assume that the τ-th burst consists of L time instants t, i.e., equivalent to a single sensing frame. The multitaper method combined with singular value decomposition was recommended for use by cognitive radios in [10]. Let us consider a number of M single-antenna sensing nodes where the received signal by the m-th node is $\mathbf{x}^{(m)}$ such that

$$\mathcal{H}_0: \quad \mathbf{x}^{(m)} = \boldsymbol{\eta}^{(m)}, \tag{38a}$$

$$\mathcal{H}_1: \quad \mathbf{x}^{(m)} = \mathbf{h}^{(m)} \odot \mathbf{s} + \boldsymbol{\eta}^{(m)}, \tag{38b}$$

where $\boldsymbol{\eta}^{(m)} \in \mathbb{C}^{L\times 1}$ and $\mathbf{h}^{(m)} \in \mathbb{C}^{L\times 1}$ are the noise and the channel vectors at the m-th node and $\mathbf{s} \in \mathbb{C}^{L\times 1}$ is the transmitted signal, such that

$$\mathbf{s} \triangleq \begin{bmatrix} s_0 & s_1 & \cdots & s_{L-1}\end{bmatrix}, \tag{39a}$$

$$\mathbf{h}^{(m)} \triangleq \begin{bmatrix} h_0^{(m)} & h_1^{(m)} & \cdots & h_{L-1}^{(m)}\end{bmatrix}, \tag{39b}$$

$$\boldsymbol{\eta}^{(m)} \triangleq \begin{bmatrix} \eta_0^{(m)} & \eta_1^{(m)} & \cdots & \eta_{L-1}^{(m)}\end{bmatrix}. \tag{39c}$$

Furthermore, let us assume that the sensing nodes are uniformly distributed inside a circle with radius r, centred on the transmitting (primary) node. It is also assumed that all nodes use the same number of Slepian vectors, which is chosen to be larger than the total number of collaborative users, i.e., $K > M$. Since each sensing node report the

local eigenspectra to the central node, then let $\mathcal{X}_k^{(m)}(f)$ be the eigenspectrum that is produced by the m-th node using the k-th Slepian sequence. Henceforth, let us define the matrix $\boldsymbol{\mathcal{A}} \in \mathbb{C}^{M\times K}$ as

$$\boldsymbol{\mathcal{A}}(f) = \begin{bmatrix} w_0^{(1)}\mathcal{X}_0^{(1)}(f) & w_1^{(1)}\mathcal{X}_1^{(1)}(f) & \dots & w_{K-1}^{(1)}\mathcal{X}_{K-1}^{(1)}(f) \\ w_0^{(2)}\mathcal{X}_0^{(2)}(f) & w_1^{(2)}\mathcal{X}_1^{(2)}(f) & \dots & w_{K-1}^{(2)}\mathcal{X}_{K-1}^{(2)}(f) \\ \vdots & \vdots & \ddots & \vdots \\ w_0^{(M)}\mathcal{X}_0^{(M)}(f) & w_1^{(M)}\mathcal{X}_1^{(M)}(f) & \dots & w_{K-1}^{(M)}\mathcal{X}_{K-1}^{(M)}(f) \end{bmatrix} \tag{40}$$

where $\omega_k^{(m)}$ is the weight assigned to the m-th user using the k-th Slepian vector. Applying SVD to the matrix $\boldsymbol{\mathcal{A}}$ produces

$$\boldsymbol{\mathcal{A}}(f) = \mathbf{U}(f)\boldsymbol{\Upsilon}(f)\mathbf{V}^{\mathrm{H}}(f), \tag{41a}$$

$$= \sum_{m=1}^{M} \sigma_m(f)\mathbf{u}_m(f)\mathbf{v}_m^{\mathrm{H}}(f), \tag{41b}$$

where the unitary matrices $\mathbf{U}$ and $\mathbf{V}$ are $M \times M$ and $K \times K$ respectively. The matrix $\boldsymbol{\Upsilon}$ is $M \times K$ and consists of the singular values $\sigma_1, \dots, \sigma_M$, $\mathbf{u}_m$ is the m-th left eigenvector and $\mathbf{v}_m$ is the associated right eigenvector[4]. Furthermore, it can be shown that [10], [34]

$$\sigma_m^2(f) = \sum_{k=0}^{K-1} \left| w_k^{(m)}\mathcal{X}_k^{(m)} \right|^2. \tag{42}$$

Within a centralized cooperative spectrum sensing context, the MTM-SVD processor requires each CR node to send its values of the eigenspectrum that were computed within a band of interest. This is represented by the m-th row of $\boldsymbol{\mathcal{A}}$. When the BS receives the various eigenspectra from all users, it constructs the matrix $\boldsymbol{\mathcal{A}}$ and applies SVD.

B. Performance of the Decision Statistic for Wideband Sensing

The decision statistic proposed in [10] can be used for wideband sensing to declare whether a frequency band is white, gray or black. Let N_{b} be the number of frequency bins, f_{low} be the lowest frequency of the bandwidth under scrutiny and Δf be the width of the frequency bin. The decision statistic is given by

$$\mathcal{I}(\tau, f) = \sum_{m=1}^{M} \sum_{l=0}^{N_{\mathrm{b}}-1} \left|\sigma_m\left(f_{\mathrm{low}} + l\,\Delta f, \tau\right)\right|^2 \Delta f. \tag{43}$$

The next step of the test to be conducted is whether the instantaneous value of the decision statistic exceeds a specific threshold for a number of N_{sb} successive bursts, i.e,

$$\bigcap_{\tau=1}^{N_{\mathrm{sb}}} \Big\{ \mathcal{I}(\tau, f) > \eta(\tau, f) \Big\}. \tag{44}$$

Looking into the previous equation and treating the decision statistic as a Hermitian form shows that the decision variable $\mathcal{I}(\tau, f)$ follows the Phase-type distribution, where the subgenerator matrix is $MKN_{\mathrm{b}} \times MKN_{\mathrm{b}}$. In this case the subgenerator matrix has the form given by (45), where the notation $\ell_{i,f}^{k,m}$ denotes the eigenvalue of the

[4]For the physical interpretation for the left singular vector and the right singular vector within the context of detection, the reader is referred to [10], [34]

This article has been accepted for publication in a future issue of this journal, but has not been fully edited. Content may change prior to final publication. Citation information: DOI 10.1109/TSP.2015.2455520, IEEE Transactions on Signal Processing

$$\mathfrak{Z}_{\mathrm{i}}^{\mathrm{SVD}} = \begin{bmatrix}
-\ell_{i,\mathfrak{f}_0}^{(0,1)} & \ell_{i,\mathfrak{f}_0}^{(0,1)} & 0 & 0 & 0 & 0 & 0 & 0 & 0 \\
0 & \ddots & \ddots & 0 & 0 & 0 & 0 & 0 & 0 \\
0 & 0 & -\ell_{i,\mathfrak{f}_{L-1}}^{(0,1)} & \ell_{i,\mathfrak{f}_{L-1}}^{(0,1)} & 0 & 0 & 0 & 0 & 0 \\
0 & 0 & 0 & -\ell_{i,\mathfrak{f}_0}^{(0,2)} & \ell_{i,\mathfrak{f}_0}^{(0,2)} & 0 & 0 & 0 & 0 \\
0 & 0 & 0 & 0 & \ddots & \ddots & 0 & 0 & 0 \\
0 & 0 & 0 & 0 & 0 & -\ell_{i,\mathfrak{f}_{L-1}}^{(0,2)} & \ell_{i,\mathfrak{f}_{L-1}}^{(0,2)} & 0 & 0 \\
0 & 0 & 0 & 0 & 0 & \ddots & \ddots & 0 & 0 \\
0 & 0 & 0 & 0 & 0 & 0 & -\ell_{i,\mathfrak{f}_0}^{(K-1,m)} & \ell_{i,\mathfrak{f}_0}^{(K-1,m)} & 0 \\
0 & 0 & 0 & 0 & 0 & 0 & \ddots & \ddots & 0 \\
0 & 0 & 0 & 0 & 0 & 0 & 0 & -\ell_{i,\mathfrak{f}_{L-2}}^{(K-1,m)} & \ell_{i,\mathfrak{f}_{L-2}}^{(K-1,m)} \\
0 & 0 & 0 & 0 & 0 & 0 & 0 & 0 & \ell_{i,\mathfrak{f}_{L-1}}^{(K-1,m)}
\end{bmatrix}, \tag{45}$$

Hermitian form representation of $\mathcal{I}(\tau, f)$ that is associated with the k-th Slepian sequence and the m-th sensing node for the f-th frequency. Finally, i refers to the considered hypothesis where $i = 0$ implies $\mathcal{H}_0$ and similarly $i = 1$ implies $\mathcal{H}_1$. Hence generalized forms for the probabilities of false alarm and missed detection are given by

$$\mathcal{P}_{\mathrm{fa}}^{\mathrm{SVD}}(\eta, \tau) = \prod_{\tau=1}^{N_{\mathrm{sb}}} \boldsymbol{\alpha}_{GLK}^{\mathrm{T}} \exp\left(\eta(\tau)\mathfrak{Z}_0^{\mathrm{SVD}}\right) \mathbf{1}_{GLK}, \tag{46a}$$

$$\mathcal{P}_{\mathrm{md}}^{\mathrm{SVD}}(\eta, \tau) = \prod_{\tau=1}^{N_{\mathrm{sb}}} 1 - \boldsymbol{\alpha}_{GLK}^{\mathrm{T}} \exp\left(\eta(\tau)\mathfrak{Z}_1^{\mathrm{SVD}}\right) \mathbf{1}_{GLK}, \tag{46b}$$

where the values of $\ell_{i,f}^{(k,m)}$ in the subgenerator matrix given by (45) are obtained by the following Theorem.

Theorem *2:* [Exact Eigenvalues of the Hermitian Form of the SVD Processor] The decision variable at the end of the τ-th burst is a Hermitian positive semidefinite form. Assuming $\mathcal{H}_0$, the eigenvalue for the m-th user and the k-th Slepian sequence at the f-th frequency (index) is

$$\ell_{0,f}^{(k,m)} = \left|w_k^{(m)}\right|^2 \sigma_n^2 \tag{47}$$

and assuming the alternate hypothesis the eigenvalue is given by

$$\ell_{1,f}^{(k,m)} = \left|w_k^{(m)}\right|^2 \left(\sigma_n^2 + \sigma_s^2 \|\mathbf{h}_m \odot \boldsymbol{\nu}^{(k,m)}(f)\|^2\right). \tag{48}$$

Proof: Similar to the employed strategy for the proof in Theorem 1, let us define the column vector $\mathbf{x}_{\mathrm{svd}}$ as given by

$$\mathbf{x}_{\mathrm{svd}} = \mathrm{vec}\Bigg(\underbrace{\mathrm{vec}\left(\mathbf{x}^{(1)} \otimes \mathbf{1}_K^{\mathrm{T}}\right), \ldots, \mathrm{vec}\left(\mathbf{x}^{(1)} \otimes \mathbf{1}_K^{\mathrm{T}}\right)}_{N_{\mathrm{b}} \text{ times}}), \ldots, \underbrace{\mathrm{vec}\left(\mathbf{x}^{(M)} \otimes \mathbf{1}_K^{\mathrm{T}}\right), \ldots, \mathrm{vec}\left(\mathbf{x}^{(M)} \otimes \mathbf{1}_K^{\mathrm{T}}\right)}_{N_{\mathrm{b}} \text{ times}})\Bigg), \tag{49}$$

and let us define the associated covariance matrix as

$$\mathbf{\Sigma}_{\rm svd} \triangleq \mathbb{E}\left[\mathbf{\underset{\sim}{x}}_{\rm svd}\mathbf{\underset{\sim}{x}}_{\rm svd}^{\rm H}\right]. \tag{50}$$

Furthermore, the decision statistic $\mathcal{I}(\tau, f)$ can be written as the Hermitian form given by

$$\mathcal{I}(\tau,f) = \mathbf{\underset{\sim}{x}}_{\rm svd}^{\rm H}\left(\bigoplus_{m=1}^{M}\bigoplus_{l=0}^{N_{\rm b}-1}\bigoplus_{k=0}^{K-1}\omega_k^{(m)^{\rm H}}\mathbf{\Psi}^{(k,m)^{\rm T}}{}_{(L,W)}\,\mathbf{\Phi}(f_{\rm low}+l\Delta f,\tau)\,\mathbf{\Psi}^{(k,m)}{}_{(L,W)}\,\omega_k^{(m)}\right)\mathbf{\underset{\sim}{x}}_{\rm svd}. \tag{51}$$

Henceforth, the property demonstrated by

$$\operatorname{rank}\left[\mathbf{\Sigma}_{\rm svd}\bigoplus_{m=1}^{M}\bigoplus_{l=0}^{N_{\rm b}-1}\bigoplus_{k=0}^{K-1}|\omega_k^{(m)}|^2\mathbf{\Psi}^{(k,m)^{\rm T}}\mathbf{\Phi}(f_{\rm low}+l\Delta f,\tau)\mathbf{\Psi}^{(k,m)}\right] = MKN_{\rm b}. \tag{52}$$

holds true since $\operatorname{rank}[\mathbf{\Sigma}_{\rm svd}] = LMKN_{\rm b}$ while $\operatorname{rank}[\mathbf{\Phi}] = 1$. Immediately, it follows that there are $MKN_{\rm b}$ nonzero eigenvalues that are associated with the Hermitian form in (51) and defined by the set

$$\begin{aligned}&\operatorname{spec}\left(\mathbf{\Sigma}_{\rm svd}\bigoplus_{m=1}^{M}\bigoplus_{l=0}^{N_{\rm b}-1}\bigoplus_{k=0}^{K-1}|\omega_k^{(m)}|^2\mathbf{\Psi}^{(k,m)^{\rm T}}\mathbf{\Phi}(f,\tau)\mathbf{\Psi}^{(k,m)}\right)\\ &\quad=\left\{\ell_{i,f}^{(k,m)} : m=1,\ldots,M,\ f=0,\ldots,N_{\rm b}-1, k=0,\ldots,K-1,\ i=0\Rightarrow\mathcal{H}_0,\ i=1\Rightarrow\mathcal{H}_1\right\}.\end{aligned} \tag{53}$$

Recalling the fact that each nonzero eigenvalue corresponds to the part of the Hermitian form that is computed by the m-th user, which is utilizing the k-th Slepian vector at the f-th frequency index, then the corresponding eigenvalue is $|\omega_k^{(m)}|^2\mathrm{tr}[\mathbf{\underset{\sim}{x}}\mathbf{\underset{\sim}{x}}^{\rm H}\mathbf{\Psi}^{(k,m)^{\rm T}}\mathbf{\Phi}(f,\tau)\mathbf{\Psi}^{(k,m)}]$ and considering $\mathcal{H}_0$ we get (47), while addressing the hypothesis $\mathcal{H}_1$ yields (48). ■

By making use of the results of the previous theorem, the probability of false alarm is reduced to

$$\mathcal{P}_{\rm fa}^{\rm SVD}(\eta,\tau) = N_{\rm b}\sum_{m=1}^{M}\sum_{k=0}^{K-1}\exp\left(\frac{-\eta(\tau)}{\sigma_n^2|w_k^{(m)}|^2}\right)\prod_{q=0,q\neq k}^{K-1}\frac{|w_q^{(m)}|^2}{|w_q^{(m)}|^2-|w_k^{(m)}|^2}, \tag{54}$$

where $\tau = 1,\ldots,N_{\rm sb}$. Similarly the probability of missed detection is given by

$$\begin{aligned}\mathcal{P}_{\rm md}^{\rm SVD}(\eta,\tau) = \prod_{\tau=1}^{N_{\rm sb}} 1 - \sum_{m=1}^{M}\sum_{l=0}^{N_{\rm b}-1}\sum_{k=0}^{K-1}\exp\left(\frac{-\eta(\tau)}{|w_k^{(m)}|^2\left(\sigma_n^2+\sigma_s^2\left\|\mathbf{\underset{\sim}{h}}^{(m)}\odot\boldsymbol{\nu}^{(k,m)}(f_l)\right\|^2\right)}\right)\\ \times\prod_{q=0,\,q\neq k}^{K-1}\frac{|w_k^{(m)}|^2\left(\sigma_n^2+\sigma_s^2\left\|\mathbf{\underset{\sim}{h}}^{(m)}\odot\boldsymbol{\nu}^{(k,m)}(f_l)\right\|^2\right)}{\sigma_n^2\left(|w_k^{(m)}|^2-|w_q^{(m)}|^2\right)+\sigma_s^2\left(|w_k^{(m)}|^2\left\|\mathbf{\underset{\sim}{h}}^{(m)}\odot\boldsymbol{\nu}^{(k,m)}(f_l)\right\|^2-|w_q^{(m)}|^2\left\|\mathbf{\underset{\sim}{h}}^{(m)}\odot\boldsymbol{\nu}^{(q,m)}(f_l)\right\|^2\right)}.\end{aligned} \tag{55}$$

C. Performance Over i.n.i.d Nakagami Channels

Different from section III-E1, in this part we assume independent but non-identical Nakagami channels. The channel envelope from the transmitting user to the m-th node is Nakagami distributed with shape and spread parameters denoted by $\mathfrak{m}_m$ and Ω_m respectively. The sensing nodes are assumed to be uniformly distributed inside a cell of radius r, centered on the transmitting primary node. In this case, the local SNR is gamma distributed where the PDF is

$$f(\gamma_t^{(m)}) = \frac{1}{\Gamma(\mathfrak{m}_m)}\left(\frac{\mathfrak{m}_m}{\overline{\gamma}^{(m)}}\right)^{\mathfrak{m}_m}\gamma_m^{\mathfrak{m}_m-1}\exp\left(-\frac{\mathfrak{m}_m}{\overline{\gamma}^{(m)}}\gamma_t^{(m)}\right). \tag{56}$$

This article has been accepted for publication in a future issue of this journal, but has not been fully edited. Content may change prior to final publication. Citation information: DOI 10.1109/TSP.2015.2455520, IEEE Transactions on Signal Processing

The average SNR (per sensing channel), i.e., $\overline{\gamma}^{(m)}$, follows a log-normal distribution with a standard deviation of θ dB, where the mean value follows a decreasing exponential path loss with exponent α_e. Hence, the PDF of the *average SNR per user*[5] $\overline{\gamma}$ can be written as [35], [36]

$$f\left(\overline{\gamma}^{(m)}\right) = \frac{2}{c}\exp\left(\frac{2\theta^2 - 2c(\overline{\gamma}^{(m)} - \overline{\gamma}_{\mathrm{rad}})}{c^2}\right) Q\left(\frac{2\theta^2 - c(\overline{\gamma}^{(m)} - \overline{\gamma}_{\mathrm{rad}})}{c\theta}\right), \tag{57}$$

where $\overline{\gamma}_{\mathrm{rad}}$ is the average SNR at distance r, $Q(\cdot)$ denote the Gaussian Q-function, $Q(z) = \frac{1}{\sqrt{2\pi}}\int_z^\infty \exp\left(-\frac{u^2}{2}\right)\,\mathrm{d}u$, and $c = 10\alpha_e \log(e)$ denotes the parameter of the exponential pass loss.

Hence, as a function of the average SNR (per user), the bound of the average probability of missed detection is obtained as given by

$$\overline{\mathcal{P}}_{\mathrm{md}}(\eta,\tau) \geq \prod_{\tau=1}^{N_{\mathrm{sb}}} 1 - \sum_{m=1}^{M}\sum_{l=0}^{N_{\mathrm{b}}-1}\sum_{k=0}^{K-1} \exp\left(\frac{-\eta(\tau)}{\sigma_n^2\omega_k^{(m)}\left(1+\mathbb{E}\left[\overline{\gamma}^{(m)}\right]\right)}\right) \prod_{q=0,q\neq i}^{K-1} \frac{\omega_k^{(m)}}{\left(\omega_k^{(m)} - \omega_q^{(m)}\right)}. \tag{58}$$

D. The Neyman-Pearson Detector over i.i.d. Nakagami Channels

Let β denote a predetermined probability of false alarm. The PDF of the decision variable assuming $\mathcal{H}_0$ and $\mathcal{H}_1$ are given by

$$f(z;\mathcal{H}_0) = \frac{1}{\Gamma(KM)}\frac{z^{KM-1}}{(\sigma_n^2)^{KM}}\exp\left(-\frac{z}{\sigma_n^2}\right), \tag{59}$$

and

$$f(z;\mathcal{H}_1) = \frac{1}{\Gamma(KM)}\frac{{\sigma_n^2}^{KM} z^{KM-1}}{(1+\overline{\gamma})^{KM}}\exp\left(\frac{-z\sigma_n^2}{1+\overline{\gamma}}\right) \tag{60}$$

respectively. Using the Neyman-Pearson criteria, the likelihood ratio test is to accept $\mathcal{H}_1$ if $\frac{f(z;\mathcal{H}_1)}{f(z;\mathcal{H}_0)}$ is larger than the threshold that yields a probability of false alarm of β. Hence the test is rewritten as

$$(1+\overline{\gamma})^{-KM}\exp\left(-\frac{z\overline{\gamma}}{\sigma_n^2(1+\overline{\gamma})}\right) \underset{\mathcal{H}_0}{\overset{\mathcal{H}_1}{\gtrless}} \eta(\beta). \tag{61}$$

Rearranging the previous equation, the modified test is

$$z \underset{\mathcal{H}_0}{\overset{\mathcal{H}_1}{\lessgtr}} -\sigma_n^2 \log\left(\eta(\beta)\left(1+\overline{\gamma}\right)^{KM}\right)\left(1+\frac{1}{\overline{\gamma}}\right). \tag{62}$$

The probability of false alarm can be inverted to obtain the value of β by utilizing the inverse regularized incomplete (upper) gamma function, $Q^{-1}(\cdot,\cdot)$, [33].

V. Impact of Noise Uncertainty

The detection of signals is affected by noise uncertainty and this issue was investigated for the conventional time-domain energy detector in many studies [37], [38]. Let α denote the noise uncertainty factor, such that the estimated noise is $\hat{\sigma}_n^2 = \alpha\sigma_n^2$. Usually the noise uncertainty factor is limited within the interval $[10^{-B/10}, 10^{B/10}]$,

[5]since here we assume identical but non-identically distributed (i.n.i.d.) fading channels, the i.i.d. case can be obtained by substituting a unified value of $\overline{\gamma}$ for $\overline{\gamma}^{(m)}$

such that in dB $10\log_{10}\alpha$ is uniformly distributed within the interval $[-B, B]$ and then the PDF of the noise uncertainty factor is given by

$$f_\alpha(z) = \begin{cases} \frac{5}{\log(10)Bz}, & 10^{-B/10} < z < 10^{B/10}, \\ 0, & \text{otherwise.} \end{cases} \tag{63}$$

Finally, the average probabilities of false alarm and detection are given by

$$\mathbb{E}\{\mathcal{P}_{\text{fa}}(\alpha)\} = \int_{10^{-B/10}}^{10^{B/10}} \mathcal{P}_{\text{fa}}(z) f_\alpha(z)\, \mathrm{d}z, \tag{64}$$

$$\mathbb{E}\{\mathcal{P}_{\text{d}}(\alpha)\} = \int_{10^{-B/10}}^{10^{B/10}} \mathcal{P}_{\text{d}}(z) f_\alpha(z)\, \mathrm{d}z, \tag{65}$$

For MIMO-MTM, closed forms for the special case of unity weights can be obtained as follows. Let us recall (30) and let us recall the substitution $\Gamma(a,b) = \Gamma(a) - \frac{b^a}{a}{}_1F_1\left(a; a+1; -b\right)$. Thus, averaging the probability of false alarm over the probability distribution of the noise uncertainty factor we get

$$\mathbb{E}\left\{\mathcal{P}_{\text{fa}}\right\} = 1 - \frac{5}{B\log(10)\Gamma(K+1)} \left(\frac{\eta K}{\sigma_n^2 M}\right)^K \int_{10^{-B/10}}^{10^{B/10}} {}_1F_1\left(K; K+1; \frac{-\eta K}{z\sigma_n^2 M}\right) z^{-K-1}\, \mathrm{d}z \tag{66}$$

which is an integral of a confluent hypergeomteric function, which can be solved into the closed form given by

$$\mathbb{E}\left\{\mathcal{P}_{\text{fa}}\right\} = 1 + \frac{5K^{-2}B^{-1}}{\Gamma(K)\log(10)} \left(\frac{K\eta}{\sigma_n^2 M}\right)^K \Bigg\{ 10^{-\frac{BK}{10}} {}_2F_2\left(\begin{matrix} K, K \\ K+1, K+1 \end{matrix}\middle| \frac{-K\eta}{\sigma_n^2 M} 10^{-\frac{B}{10}}\right) - 10^{\frac{BK}{10}} {}_2F_2\left(\begin{matrix} K, K \\ K+1, K+1 \end{matrix}\middle| \frac{-K\eta}{\sigma_n^2 M} 10^{\frac{B}{10}}\right) \Bigg\} \tag{67}$$

where

$${}_pF_q\left(a_1, \ldots, a_p; b_1, \ldots, b_q; z\right) = \sum_{k=0}^{\infty} \frac{1}{k!} \frac{(a_1)_k (a_2)_k \ldots (a_p)_k}{(b_1)_k (b_2)_k \ldots (b_q)_k} z^k$$

is generalized hypergeometric function and for brevity we use

$${}_pF_q\left(a_1, \ldots, a_p; b_1, \ldots, b_q; z\right) = {}_pF_q\left(\begin{matrix} a_1, \ldots, a_p \\ b_1, \ldots, b_q \end{matrix}\middle| z\right).$$

Using the same procedure the average probability of detection can be obtained. Let $g = \frac{K\eta}{\sigma_n^2 M}$, $c = \frac{\Omega\sigma_s^2}{\sigma_n^2}$, $b = 10^{\frac{B}{10}}$ and $a = 10^{-\frac{B}{10}}$. Recalling (34), the average probability of detection is expressed by the integral in

$$\mathbb{E}\left\{\mathcal{P}_{\text{d}}\right\} = 1 - \frac{5}{B\log(10)\Gamma(K+1)} \int_{10^{-B/10}}^{10^{B/10}} \frac{1}{z} \left(\frac{\eta K}{z\sigma_n^2 M + \sigma_s^2 \Omega M}\right)^K {}_1F_1\left(K; K+1; \frac{-\eta K}{z\sigma_n^2 M + \sigma_s^2 \Omega M}\right) \mathrm{d}z \tag{68}$$

This article has been accepted for publication in a future issue of this journal, but has not been fully edited. Content may change prior to final publication. Citation information: DOI 10.1109/TSP.2015.2455520, IEEE Transactions on Signal Processing

which can be solved as

$$\mathbb{E}\left\{\mathcal{P}_{\rm d}\right\} = 1 + \frac{5K^{-2}B^{-1}g^{K}c^{K-2}}{\Gamma(K)\log(10)(K-1)} \times \left\{ \left(\frac{c}{a+c}\right)^{K-1} \mathbf{F}^{1:1;1}_{1:1;0}\left(\begin{matrix} K-1: & K & ;1; \\ K & :K+1 & ;-; \end{matrix} \middle| -\frac{g}{a+c}, \frac{c}{a+c} \right) - \left(\frac{c}{b+c}\right)^{K-1} \mathbf{F}^{1:1;1}_{1:1;0}\left(\begin{matrix} K-1: & K & ;1; \\ K & :K+1 & ;-; \end{matrix} \middle| -\frac{g}{b+c}, \frac{c}{b+c} \right) \right\}, \quad (69)$$

where the function $\mathbf{F}(\cdot)$ is Kampé de Fériet function where the function definition and the full proof are provided in the Appendix.

VI. Simulation Results and Discussion

In this section we provide simulation results and numerical examples to give an insight into the performance of the multitaper method for the two considered scenarios of MIMO-MTM and MTM-SVD. Fig. 2 validates the accuracy of the derived formulas for the PDF of the decision variable under the hypotheses $\mathcal{H}_0$ and $\mathcal{H}_1$ for both cases of MIMO-MTM and the MTM-SVD processor. It is obvious that by using the derived parameters for the Phase-Type probability distribution, the theoretical probability distribution functions are matching for both cases of the null hypothesis $\mathcal{H}_0$ and the alternate hypothesis $\mathcal{H}_1$. The results were obtained using a sample size of 64 and a number of 4 DPSSs. For the case of MIMO-MTM, the transmitter employs a number of $N = 3$ transmit antennas, while the receiver employs a number of $M = 4$ antennas. For the case of MTM-SVD, the number of cooperating nodes is $M = 3$.

Fig. 3 presents a comparison between MIMO-MTM and all other nonparametric power spectrum estimators: the periodogram, Bartlett's method and Welch's method. The performance comparison is provided in terms of the receiver operating characteristics (ROC), i.e., the probability of detection versus the probability of false alarm. For Bartlett's method the vector $\breve{\mathbf{x}}$ is divided into $K_{\rm B}$ sub-segments each of length $L_{\rm B}$. For Welch's method, an overlapping factor, ϵ, is used to divide $\breve{\mathbf{x}}$ into a number of overlapping segments each of length $L_{\rm w}$, such that the resultant number of segments is $K_{\rm w}$. Hence, based on the assumed MIMO structure, the periodogram, Bartlett's estimate and Welch's estimate are given by

$$\hat{\mathcal{S}}_x(f) = \frac{1}{L}\left|\sum_{t=0}^{L-1} \breve{x}(t) e^{-j2\pi ft/L}\right|^2, \quad (70)$$

$$\hat{\mathcal{S}}_x^{\rm Bart}(f) = \frac{1}{K_{\rm B}L_{\rm B}}\sum_{i=1}^{K_{\rm B}}\left|\sum_{t=0}^{L_{\rm B}-1} \breve{x}(t) e^{-j2\pi ft/L_{\rm B}}\right|^2, \quad (71)$$

This article has been accepted for publication in a future issue of this journal, but has not been fully edited. Content may change prior to final publication. Citation information: DOI 10.1109/TSP.2015.2455520, IEEE Transactions on Signal Processing

$$\hat{\mathbb{S}}_x^{\mathrm{WOSA}}(f)= \frac{1}{K_{\mathrm{w}}L_{\mathrm{w}}}\sum_{i=1}^{K_{\mathrm{w}}}\left|\sum_{t=0}^{L_{\mathrm{w}}-1}\breve{x}(t+i\epsilon)e^{-j2\pi ft/L_{\mathrm{w}}}\right|^2, \tag{72}$$

where $\hat{\mathbb{S}}_x$, $\hat{\mathbb{S}}_x^{\mathrm{Bart}}$ and $\hat{\mathbb{S}}_x^{\mathrm{WOSA}}$ denote the periodogram, Bartlett's estimator and Welch's estimator respectively. The values of the sub-segemnt parameters K_{B} and K_{W} are obtained as a function of L as:

$$\begin{cases} K_{\mathrm{B}} = \frac{L}{L_{\mathrm{B}}}, \\ K_{\mathrm{W}} = \frac{L-\epsilon}{L_{\mathrm{W}}-\epsilon}, \end{cases} \tag{73}$$

respectively.

The simulation parameters are $L = 16$, $M = 5$, $N = 3$, $K = 6$, $K_{\mathrm{B}} = K_{\mathrm{W}} = 2$, $\epsilon = 4$. From Fig. 3, it can be seen that MIMO-MTM yields the best performance compared to all other nonparametric methods. Both Bartlett and Welch's methods yield the same ergodic probability of detection as long as $K_{\mathrm{W}} = K_{\mathrm{B}}$, and therefore they both yield the same ROC curves as shown in the figure. The periodogram yields the poorest performance, as it yields the lowest probability of detection for a given probability of false alarm.

In Fig. 4, its shown that applying the Neyman-Pearson approach introduces further enhancement in the performance of MIMO-MTM for low values of the SNR. The figure illustrates the receiver operator characteristics for two values of the SNR, given by -11dB and -25dB, respectively. The simulation parameters are $N = 3$ transmit antennas, $M = 5$ receive antennas, the length of the sensing frame is $L = 256$ samples and the number of DPSSs is $K = 16$. The optimized detection threshold is given in (36). It can be seen that the performance is significantly enhanced, as the average probability of detection is maximized as a function of the probability of false alarm.

Table I presents a comparison between the MIMO-MTM model and other nonparametric methods. The table provides numerical examples which demonstrate the performance in terms of the probability of detection and the probability of missed detection for predefined values of the probability of false alarm given by $\mathcal{P}_{\mathrm{fa}} = \{0.05, 0.1, 0.2\}$. These values where chosen as spectrum sensing techniques are optimally required to have a maximum probability of false alarm of 0.1, and a minimum probability of detection of 0.9 [39]. The results presented in the table contains both MIMO-MTM and MIMO-MTM combined with the Neyman-Pearson approach from Section III-E2 using the likelihood ratio in (36). Generally, for small values of the SNR, the performance of most detectors tend to lie on the line-of-no-discrimination. For example, from the table it can be seen that for a small SNR of -17dB and -9dB, the periodogram produces an achievable pair ($\mathcal{P}_{\mathrm{fa}}$, $\mathcal{P}_{\mathrm{md}}$), that lies in the line-of-no-discrimination (this effect is also shown in Fig.3). However, with optimization using the NPA, the ergodic probability of detection is maximized and the performance of MIMO-MTM is significantly enhanced as can be seen from the numerical values in the table. In fact, MIMO-MTM succeeded on satisfying the constraint of the probability of false alarm, while reducing the probability of miss as well.

Fig. 5 illustrates the average probability of detection versus the number of samples within a single sensing frame. The figure compares between MIMO-MTM, the periodogram, Bartlett's method and Welch's method. For a given sample size, MIMO-MTM outperforms all other methods. It can also be seen that MIMO-MTM, Bartlett's method and Welch's method are not affected by any increase in the sample size and provides a constant average probability

of detection. However, the periodogram is affected by low sample sizes and the performance converges to a constant value as the sample size increases.

Fig. 6 depicts the effect of noise uncertainty when using MIMO-MTM. The results show that the expressions obtained in Section V are accurate. The simulation parameters are $\mathfrak{m} = 1$, $\Omega = 0.5$, $N = 3$, $M = 5$, for two cases: 1) $\sigma_s^2 = 1.5$, $\sigma_n^2 = 2$, total SNR= -4.2597dB and 2) $\sigma_s^2 = 4$, $\sigma_n^2 = 10$, total SNR= 4dB. A worst case is assumed of $B = 2$dB. It is also shown that the performance margin is very negligible, which makes the performance identical to the case of when the impact of noise uncertainty is ignored.

Fig.7 shows the receiver operator characteristics assuming that the fading process is independent but not identically distributed. The MTM-SVD procssor is also compared with the case of using periodograms. A number of $M = \{4, 6, 8\}$ sensing nodes are assumed, where each sensing node uses a $K = 16$ Slepian vectors. The local weights are assumed to be the energy concentrations of the Slepian vectors. The average SNR of a distance equivalent to the radius from the primary transmitting node is $\overline{\gamma}_{\mathrm{rad}} = 6$ dB and $\alpha_e = 3.5$. It can be seen that when the probability of false alarm is 0.1, almost all cases yield a probability of detection of 1.

Finally, in Fig. 8 we plot the average probability of detection versus the SNR when the threshold is optimized to maximize the probability of detection assuming independent and identically distributed fading channels with $\overline{\gamma} = 6$ dB. The optimized threshold is given by (61). Simulations were carried for $M = 5$, $K = 16$ and two cases of number of frequency bins and it can be seen that using a larger number of bins yields better performance.

VII. Conclusion

This study set out to determine the exact performance analysis of the multitaper detector from two perspectives: MIMO-MTM and the MTM-SVD processor. Both multitaper-based scenarios were investigated within the context of detection of primary transmissions over fading channels, for nodes that employ opportunistic spectrum access. This study has shown that the decision variable for both considered scenarios can be statistically modeled using the Phase-Type distribution, where the exact distribution parameters were derived as the nonzero eigenvalues of the Hermitian form representations of the corresponding variables. The findings showed that in general the derived analytical results accurately matched the investigated scenarios. Furthermore, in this paper, we extended the obtained models into optimized versions using the Neyman-Pearson Approach over Nakagami channels. Finally, we also investigated the impact of noise uncertainty in a MIMO-MTM node. As a summary, for the case of MIMO-MTM, the performance is significantly enhanced by increasing the number of Slepian vectors and number of receiving antennas, and MIMO-MTM is robust under noise uncertainty. For the case of the MTM-SVD processor, the performance is a function of the number of collaborating nodes, frequency resolution and number of Slepian vectors as well. It is mention worthy that the obtained models in this paper provides a basis for further optimization investigations for the MTM.

Appendix

This article has been accepted for publication in a future issue of this journal, but has not been fully edited. Content may change prior to final publication. Citation information: DOI 10.1109/TSP.2015.2455520, IEEE Transactions on Signal Processing

Let $g=\frac{K\eta}{\sigma_n^2 M}$ and $c=\frac{\Omega\sigma_s^2}{\sigma_n^2}$. Let us consider the integral of the form

$$\mathcal{J}=\frac{g^K}{K}\int_a^b {}_1F_1\left(\begin{matrix}K\\K+1\end{matrix}\Big|\frac{-g}{z+c}\right)z^{-1}\left(z+c\right)^{-K}\,\mathrm{d}z, \tag{74}$$

which can be expressed as

$$\mathcal{J}=\frac{g^K}{Kc^{K-1}}\int_{\frac{c}{b+c}}^{\frac{c}{a+c}} {}_1F_1\left(\begin{matrix}K\\K+1\end{matrix}\Big|-\frac{g}{c}y\right)\times y^{K-2}\left(1-y\right)^{-1}\,\mathrm{d}y, \tag{75}$$

which yields

$$\mathcal{J}=\frac{g^K}{Kc^{K-1}}\left\{\mathbf{\Delta}\left(\frac{c}{a+c}\right)-\mathbf{\Delta}\left(\frac{c}{b+c}\right)\right\}, \tag{76}$$

where

$$\mathbf{\Delta}(z)=\frac{z^{K-2}}{K-2}\mathbf{F}\,{}^{1:1;1}_{1:1;0}\left(\begin{matrix}K-2:\quad K\quad;1\;;\\K-1:K+1\;;-\;;\end{matrix}\Big|-\frac{g}{c}z,z\right) \tag{77}$$

which is the notation for the Kampé de Fériet function introduced by Srivastava and Panda and reported in [40] as:

$$\mathbf{F}\,{}^{\boldsymbol{A}:\boldsymbol{B};\boldsymbol{C}}_{\check{\boldsymbol{A}}:\check{\boldsymbol{B}};\check{\boldsymbol{C}}}\left(\begin{matrix}(\boldsymbol{a}):(\boldsymbol{b})\;;(\boldsymbol{c})\;;\\(\check{\boldsymbol{a}}):(\check{\boldsymbol{b}})\;;(\check{\boldsymbol{c}})\;;\end{matrix}\Big|y,z\right)=\sum_{s=0}^{\infty}\sum_{r=0}^{\infty}\frac{1}{r!}\frac{1}{s!}\frac{(\boldsymbol{a})_{r+s}(\boldsymbol{b})_r(\boldsymbol{c})_s}{(\check{\boldsymbol{a}})_{r+s}(\check{\boldsymbol{b}})_r(\check{\boldsymbol{c}})_s}y^r z^s, \tag{78}$$

where

$$(\boldsymbol{a})_n=(a_1)_n(a_2)_n\ldots(a_{\boldsymbol{A}})_n, \tag{79a}$$

$$(\boldsymbol{b})_n=(b_1)_n(b_2)_n\ldots(b_{\boldsymbol{B}})_n, \tag{79b}$$

$$(\boldsymbol{c})_n=(c_1)_n(c_2)_n\ldots(c_{\boldsymbol{C}})_n, \tag{79c}$$

$$(\check{\boldsymbol{a}})_n=(\check{a}_1)_n(\check{a}_2)_n\ldots(\check{a}_{\check{\mathbf{A}}})_n, \tag{79d}$$

$$(\check{\boldsymbol{b}})_n=(\check{b}_1)_n(\check{b}_2)_n\ldots(\check{b}_{\check{\mathbf{B}}})_n, \tag{79e}$$

$$(\check{\boldsymbol{c}})_n=(\check{c}_1)_n(\check{c}_2)_n\ldots(\check{c}_{\check{\mathbf{C}}})_n, \tag{79f}$$

where $(\cdot)_n$ is Pochhammer symbol.

REFERENCES

[1] J. Mitola and J. Maguire, G.Q., "Cognitive radio: making software radios more personal," *IEEE Pers Commun*, vol. 6, no. 4, pp. 13–18, 1999.

[2] J. Mitola, *Cognitive Radio Architecture: The Engineering Foundations of Radio XML*. Wiley, october 2006.

[3] D. Niyato, E. Hossain, and Z. Han, "Dynamic spectrum access in ieee 802.22- based cognitive wireless networks: a game theoretic model for competitive spectrum bidding and pricing," *IEEE Wireless Communications*, vol. 16, no. 2, pp. 16–23, April 2009.

[4] ECC REPORT 205, "Licensed Shared Access (LSA)," ECC, Tech. Rep., february 2014.

[5] IEEE 802.22 Working Group on Wireless Regional Area Networks. [Online]. Available: http://www.ieee802.org/22/

[6] E. Axell, G. Leus, E. G. Larsson, and H. V. Poor, "Spectrum sensing for cognitive radio : State-of-the-art and recent advances," *IEEE Signal Processing Mag.*, vol. 29, no. 3, pp. 101–116, 2012.

[7] T. Yucek and H. Arslan, "A survey of spectrum sensing algorithms for cognitive radio applications," *IEEE Communications Surveys & Tutorials*, vol. 11, no. 1, pp. 116–130, 2009.

[8] R. Umar, A. U. H. Sheikh, and M. Deriche, "Unveiling the hidden assumptions of energy detector based spectrum sensing for cognitive radios," *IEEE Communications Surveys & Tutorials*, vol. 16, no. 2, pp. 713–728, 2014.

[9] A. Kortun, T. Ratnarajah, M. Sellathurai, Y. Liang, and Y. Zeng, "On the eigenvalue-based spectrum sensing and secondary user throughput," *IEEE Trans. Veh. Technol.*, vol. 63, no. 3, pp. 1480–1486, 2014.

[10] S. Haykin, "Cognitive radio: brain-empowered wireless communications," *IEEE J. Select. Areas Commun.*, vol. 23, no. 2, pp. 201–220, 2005.

[11] D. B. Percival and A. T. Walden, *Spectral Analysis for Physical Applications:Multitaper and Conventional Univariate Techniques*. Cambridge University Press, 1993.

[12] D. Slepian, "Prolate spheroidal wave functions, fourier analysis, and uncertaintyv: The discrete case," *Bell System Technical Journal*, vol. 57, no. 5, pp. 1371–1430, 1978.

[13] B. Farhang-Boroujeny, "Filter bank spectrum sensing for cognitive radios," *IEEE Trans. Signal Processing*, vol. 56, no. 5, pp. 1801–1811, 2008.

[14] E. H. Gismalla and E. Alsusa, "Performance analysis of the periodogram-based energy detector in fading channels," *IEEE Trans. Signal Processing*, vol. 59, no. 8, pp. 3712–3721, 2011.

[15] ——, "On the performance of energy detection using bartlett's estimate for spectrum sensing in cognitive radio systems," *IEEE Transactions on Signal Processing*, vol. 60, no. 7, pp. 3394–3404, 2012.

[16] ——, "On the detection of unknown signals using Welch overlapped segmented averaging method," in *IEEE Vehicular Technology Conference (VTC Fall)*, 2011, pp. 1–5.

[17] E. Gismalla and E. Alsusa, "New and accurate results on the performance of the multitaper-based detector," in *IEEE International Conference on Communications (ICC)*, June 2012, pp. 1609–1613.

[18] E. H. G. Yousif and E. Alsusa, "A new and generalized model for the multitaper detector with nonzero mean signals," to appear in Globecom 2014 - Cognitive Radio and Networks Symposium (GC14 CogRN), Austin, USA, Dec. 2014.

[19] O. A. Alghamdi and M. Abu-Rgheff, "Performance evaluation of cognitive radio spectrum sensing using multitaper-singular value decomposition," in *4th International Conference on Cognitive Radio Oriented Wireless Networks and Communications*, June 2009, pp. 1–6.

[20] Q. T. Zhang, "Theoretical performance and thresholds of the multitaper method for spectrum sensing," *IEEE Trans. Veh. Technol.*, vol. 60, no. 5, pp. 2128–2138, 2011.

[21] D. Slepian, "Prolate spheriodal wave functions, fourier analysis and uncertainty," *Bell syst. Tech. J.*, vol. 57, pp. 1371–1430, 1978.

[22] S. Haykin, *Cognitive Dynamic Systems: Perception-action Cycle, Radar and Radio*. Cambridge University Press, march 2012.

[23] ——, *Fundamental Issues in Cognitive Radio*. Springer, 2007, ch. 1.

[24] A. M. Mathai and S. B. Provost, *Quadratic forms in random variables*.

[25] M. Simon, *Probability distributions involving Gaussian random variables: A handbook for engineers and scientists*. Springer Netherlands, 2002.

[26] M. F. Neuts, *Matrix-geometric Solutions in Stochastic Models: An Algorithmic Approach*. Courier Dover Publications, 1995.

[27] W. J. Stewart, *Probability, Markov Chains, Queues, and Simulation: The Mathematical Basis of Performance Modeling*. Woodstock, Oxfordshire, UK: Princeton University Press, 2009.

[28] P. Buchholz, *Input Modeling with Phase-Type Distributions and Markov Models: Theory and Applications*, ser. Springer Briefs in Mathematics. Springer, 2014.

[29] K. Al-Begain, D. Fiems, and J. Vincent, *Analytical and Stochastic Modeling Techniques and Applications: 19th International Conference, ASMTA 2012, Grenoble, France, June 4-6, 2012. Proceedings*, ser. Lecture Notes in Computer Science. Springer Berlin Heidelberg, 2012.

[30] I. S. Gradshteyn and I. M. Ryzhik, *Table of Integrals, Series, and Products*, 7th ed., A. Jeffrey and D. Zwillinger, Eds. Academic Press, 2007.

[31] R. Hippenstiel, *Detection Theory: Applications and Digital Signal Processing*. Taylor & Francis, 2001.

[32] J. D. Gibson and J. L. Melsa, *Introduction to Nonparametric Detection with Applications*. Academic Press, 1976.

[33] A. R. DiDonato and A. H. Morris Jr, "Computation of the incomplete gamma function ratios and their inverse," *ACM Transactions on Mathematical Software (TOMS)*, vol. 12, no. 4, pp. 377–393, 1986.

[34] S. Haykin, D. J. Thomson, and J. H. Reed, "Spectrum sensing for cognitive radio," *Proc. IEEE*, vol. 97, no. 5, pp. 849–877, 2009.

[35] A. Rao and M.-S. Alouini, "Performance of cooperative spectrum sensing over non-identical fading environments," *IEEE Transactions on Communications*, vol. 59, no. 12, pp. 3249–3253, Dec 2011.

[36] M. Yacoub, *Foundations of Mobile Radio Engineering*. CRC Press Inc., 1993.

[37] A. Mariani, A. Giorgetti, and M. Chiani, "Effects of noise power estimation on energy detection for cognitive radio applications," *IEEE Trans. Commun.*, vol. 59, no. 12, pp. 3410–3420, 2011.

[38] R. Tandra and A. Sahai, "SNR walls for signal detection," vol. 2, no. 1, pp. 4–17, 2008.

[39] C. R. Stevenson, C. Cordeiro, E. Sofer, and G. Chouinard, "IEEE P802.22 Wireless RANs Functional Requirements for the 802.22 WRAN Standard doc.:IEEE 802.22-05/0007r46, Submission by Carl R. Stevenson," pp. 1–49, Sept 2005.

[40] H. M. Srivastava and P. W. Karlsson, *Multiple Gaussian hypergeometric series*. E. Horwood, 1985.

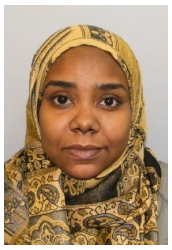

Ebtihal Yousif (S'10-M'13), received the B.Sc. degree with Honours in Electronic Engineering in 2003 and the M.Sc. degree in 2007 from Sudan University of Science and Technology (SUST). From 2005 to June 2007 she served as a teaching assistant and then she worked as a lecturer till December 2008 in the Electronic Engineering department in SUST. In 2009, She joined the Microwave and Communications Systems (MACS) group of the University of Manchester where she worked as part-time staff and received her P.hD degree in 2013. She is currently a research fellow within the FP7 project ADEL (3.7M€) in the area of licensed shared access. Her primary research interests are in wireless communication systems including next generation technologies, dynamic spectrum access, statistical signal processing, information theoretic aspects, MIMO systems and applications of machine learning for wireless systems.

Tharmalingam Ratnarajah (A'96-M'05-SM'05) is currently with the Institute for Digital Communications, University of Edinburgh, Edinburgh, UK, as a Professor in Digital communications and signal processing. His research interests include signal processing and information theoretic aspects of 5G wireless networks, full-duplex radio, mmWave communications, random matrices theory, interference alignment, statistical and array signal processing and quantum information theory. He has published over 250 publications in these areas and holds four U.S. patents. He is currently the coordinator of the FP7 projects HARP (3.2M€) in the area of highly distributed MIMO and ADEL (3.7M€) in the area of licensed shared access. Previously, he was the coordinator of FP7 Future and Emerging Technologies project CROWN (2.3M€) in the area of cognitive radio networks and HIATUS (2.7M€) in the area of interference alignment. Dr Ratnarajah is a Fellow of Higher Education Academy (FHEA), U.K., and an associate editor of the IEEE Transactions on Signal Processing.

Mathini Sellathurai (S'95-M'02-SM'06) is presently a Reader with the Heriot-Watt University, Edinburgh, U.K and leading research in signal processing for intelligent systems and wireless communications. Her research includes adaptive, cognitive and statistical signal processing techniques in a range of applications including Radar and RF networks, Network Coding, Cognitive Radio, MIMO signal processing, satellite communications and ESPAR antenna communications. She has been active in the area of signal processing research for the past 15 years and has a strong international track record in multiple-input, multiple-output (MIMO) signal processing with applications in radar and wireless communications research. Dr. Sellathurai has 5 years of industrial research experience. She held positions with Bell-Laboratories, New Jersey, USA, as a visiting researcher (2000); and with the Canadian (Government) Communications Research Centre, Ottawa Canada as a Senior Research Scientist (2001-2004). Since 2004 August, she has been with academia. She also holds an honorary Adjunct/Associate Professorship at McMaster University, Ontario, Canada, and an Associate Editorship for the IEEE Transactions on Signal Processing between 2009 -2013 and presently serving as an IEEE SPCOM Technical Committee member. She has published over 150 peer reviewed papers in leading international journals and IEEE conferences; given invited talks and written several book chapters as well as a research monograph titled Space-Time Layered Processing as a lead author. The significance of her accomplishments is recognized through international awards, including an IEEE Communication Society Fred W. Ellersick Best Paper Award in 2005, Industry Canada Public Service Awards for contributions in science and technology in 2005 and awards for contributions to technology Transfer to industries in 2004. Dr. Sellathurai was the recipient of the Natural Sciences and Engineering Research Council of Canadas doctoral award for her Ph.D. dissertation.

This article has been accepted for publication in a future issue of this journal, but has not been fully edited. Content may change prior to final publication. Citation information: DOI 10.1109/TSP.2015.2455520, IEEE Transactions on Signal Processing

TABLE I

NUMERICAL EXAMPLES FOR COMPARISON BETWEEN MIMO-MTM AND OTHER NONPARAMETRIC ESTIMATORS

		MIMO-MTM (with NPA)		MIMO-MTM		Welch		Bartlett		Periodogram	
		$L=16$,$K=16$				$L=16$, $K_{\mathrm{W}}=2$, $\epsilon=4$, $L_{\mathrm{B}}=10$		$L=16$, $K_{\mathrm{B}}=2$ $L_{\mathrm{B}}=8$		$L=16$	
$M=3$,$N=2$	$\mathcal{P}_{\mathrm{fa}}$	$\mathcal{P}_{\mathrm{d}}$	$\mathcal{P}_{\mathrm{md}}$	$\mathcal{P}_{\mathrm{d}}$	$\mathcal{P}_{\mathrm{md}}$	$\mathcal{P}_{\mathrm{d}}$	$\mathcal{P}_{\mathrm{md}}$	$\mathcal{P}_{\mathrm{d}}$	$\mathcal{P}_{\mathrm{md}}$	$\mathcal{P}_{\mathrm{d}}$	$\mathcal{P}_{\mathrm{md}}$
Rayleigh SNR=-17dB	0.05	1	0	0.06	0.940	0.054	0.946	0.054	0.946	0.050	0.950
	0.1	1	0	0.116	0.884	0.106	0.894	0.106	0.894	0.100	0.900
	0.2	1	0	0.224	0.776	0.209	0.791	0.209	0.791	0.200	0.800
Nakagami m=6 SNR=-9dB	0.05	1	0	0.124	0.876	0.076	0.924	0.076	0.924	0.051	0.949
	0.1	1	0	0.210	0.790	0.139	0.861	0.139	0.861	0.100	0.900
	0.2	1	0	0.350	0.650	0.254	0.746	0.254	0.746	0.202	0.708

This article has been accepted for publication in a future issue of this journal, but has not been fully edited. Content may change prior to final publication. Citation information: DOI 10.1109/TSP.2015.2455520, IEEE Transactions on Signal Processing

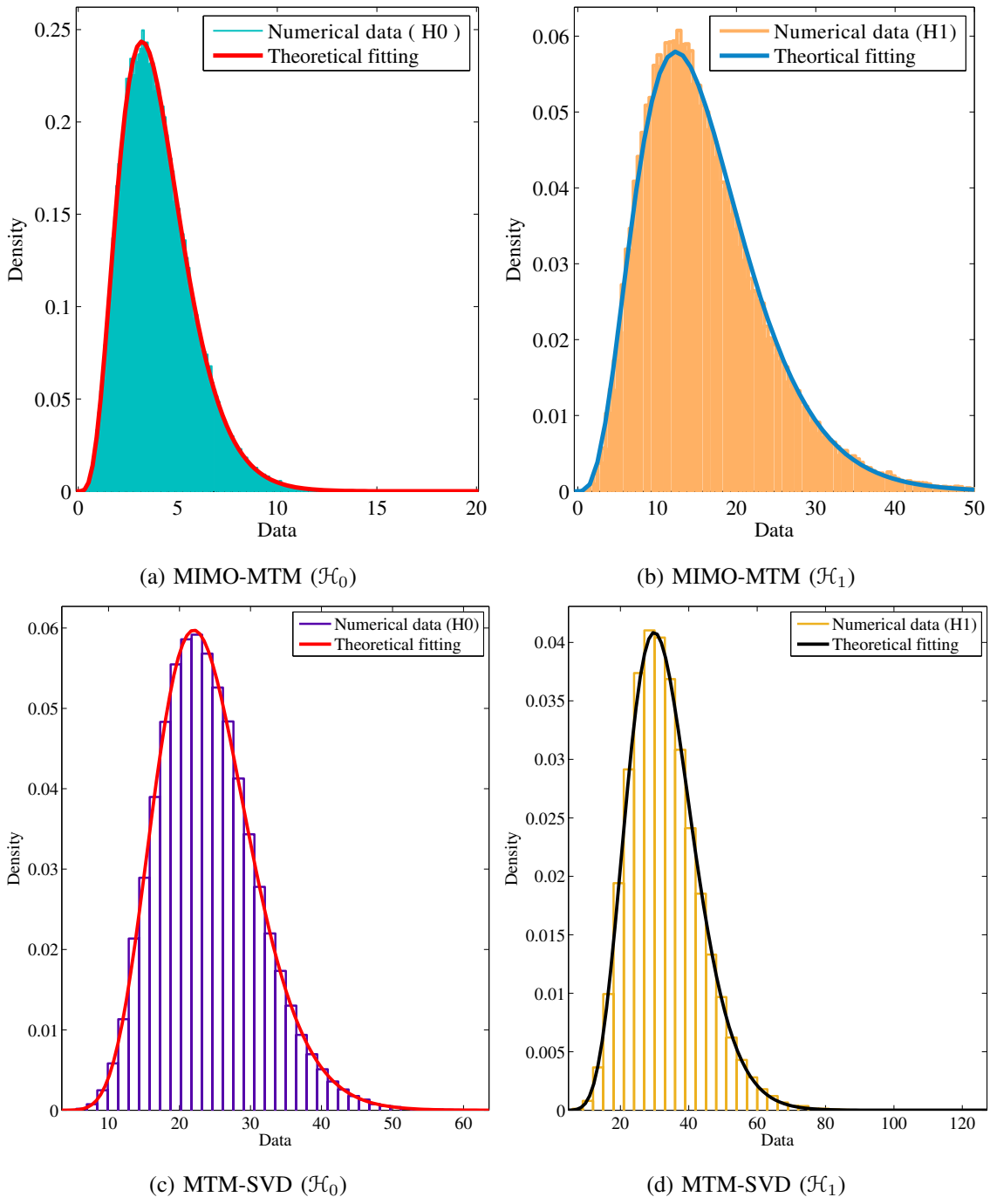

(a) MIMO-MTM ($\mathcal{H}_0$) (b) MIMO-MTM ($\mathcal{H}_1$)

(c) MTM-SVD ($\mathcal{H}_0$) (d) MTM-SVD ($\mathcal{H}_1$)

Fig. 2. Fitting of Phase-Type theoretical PDFs of the decision variable and numerical data for both MIMO-MTM and MTM-SVD.

This article has been accepted for publication in a future issue of this journal, but has not been fully edited. Content may change prior to final publication. Citation information: DOI 10.1109/TSP.2015.2455520, IEEE Transactions on Signal Processing

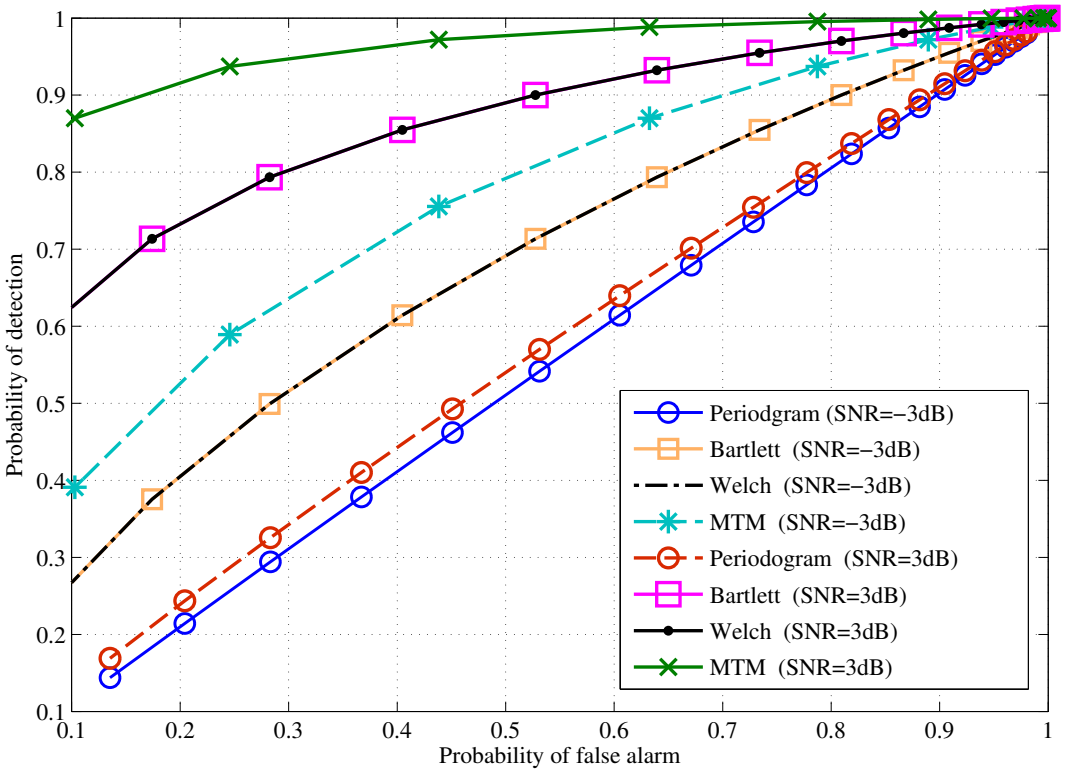

Fig. 3. Comparison between MIMO-MTM and the case of using MIMO with other nonparametric PSD estimators ($K = 4$, $L = 16$, $M = 5$, $N = 3$)

This article has been accepted for publication in a future issue of this journal, but has not been fully edited. Content may change prior to final publication. Citation information: DOI 10.1109/TSP.2015.2455520, IEEE Transactions on Signal Processing

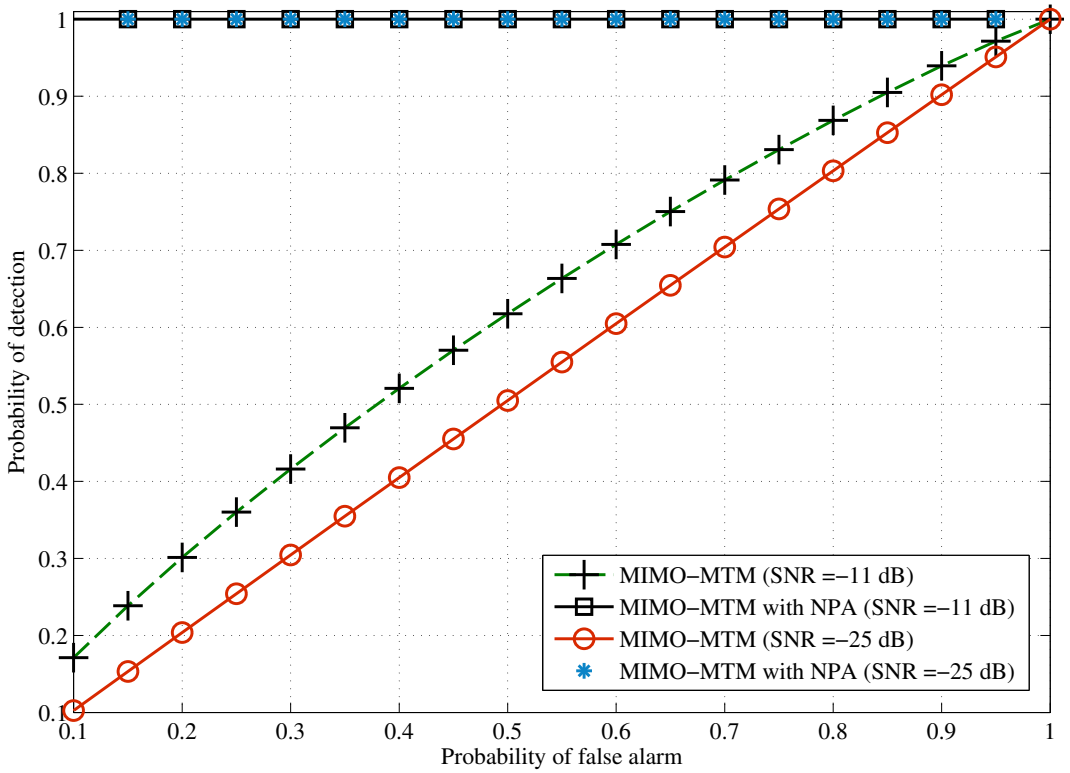

Fig. 4. Further enhancement of MIMO-MTM using the Neyman Pearson Approach (NPA) in law values of the SNR. ($K = 16$, $L = 256$, $M = 5$, $N = 3$)

This article has been accepted for publication in a future issue of this journal, but has not been fully edited. Content may change prior to final publication. Citation information: DOI 10.1109/TSP.2015.2455520, IEEE Transactions on Signal Processing

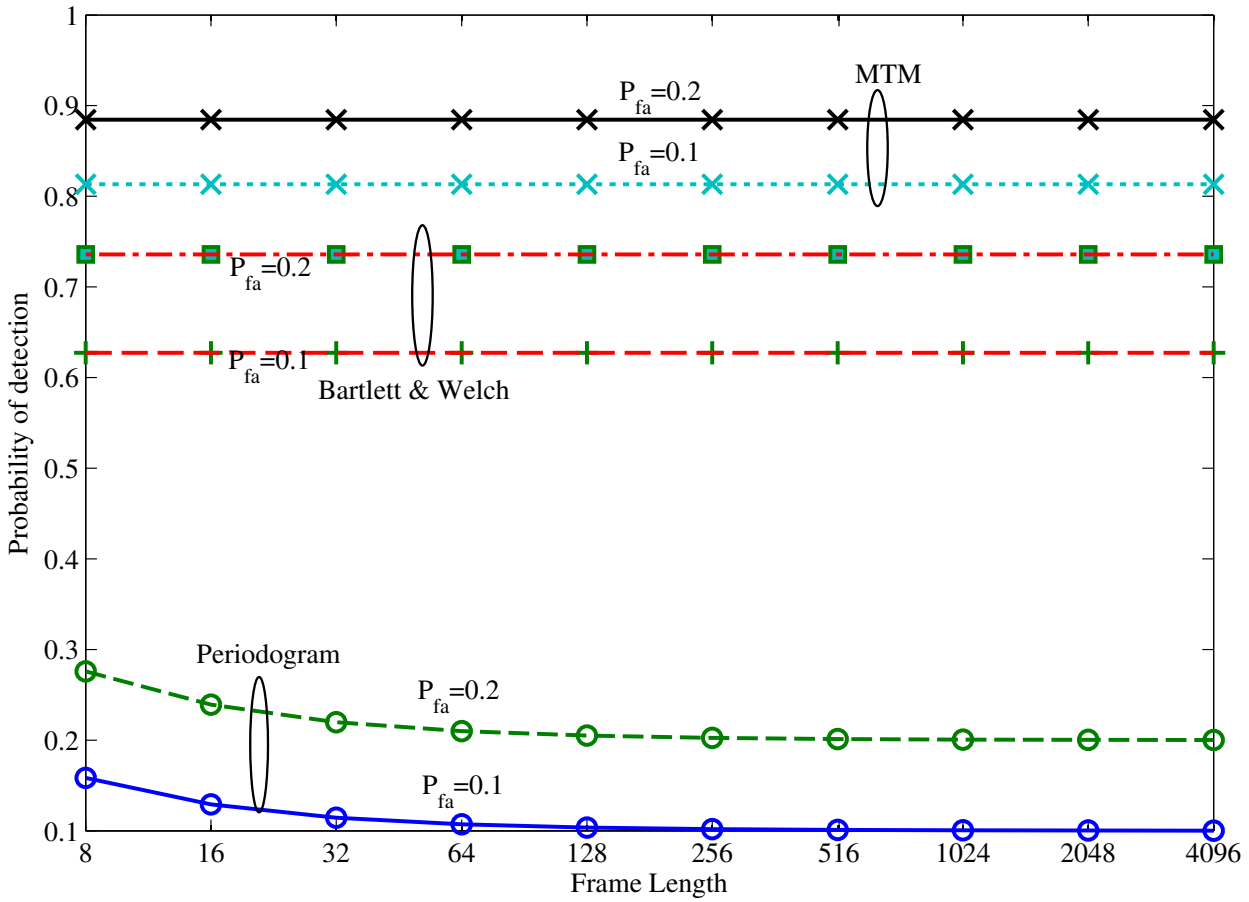

Fig. 5. Comparison between all nonparametric methods based on the impact of the sensing frame

This article has been accepted for publication in a future issue of this journal, but has not been fully edited. Content may change prior to final publication. Citation information: DOI 10.1109/TSP.2015.2455520, IEEE Transactions on Signal Processing

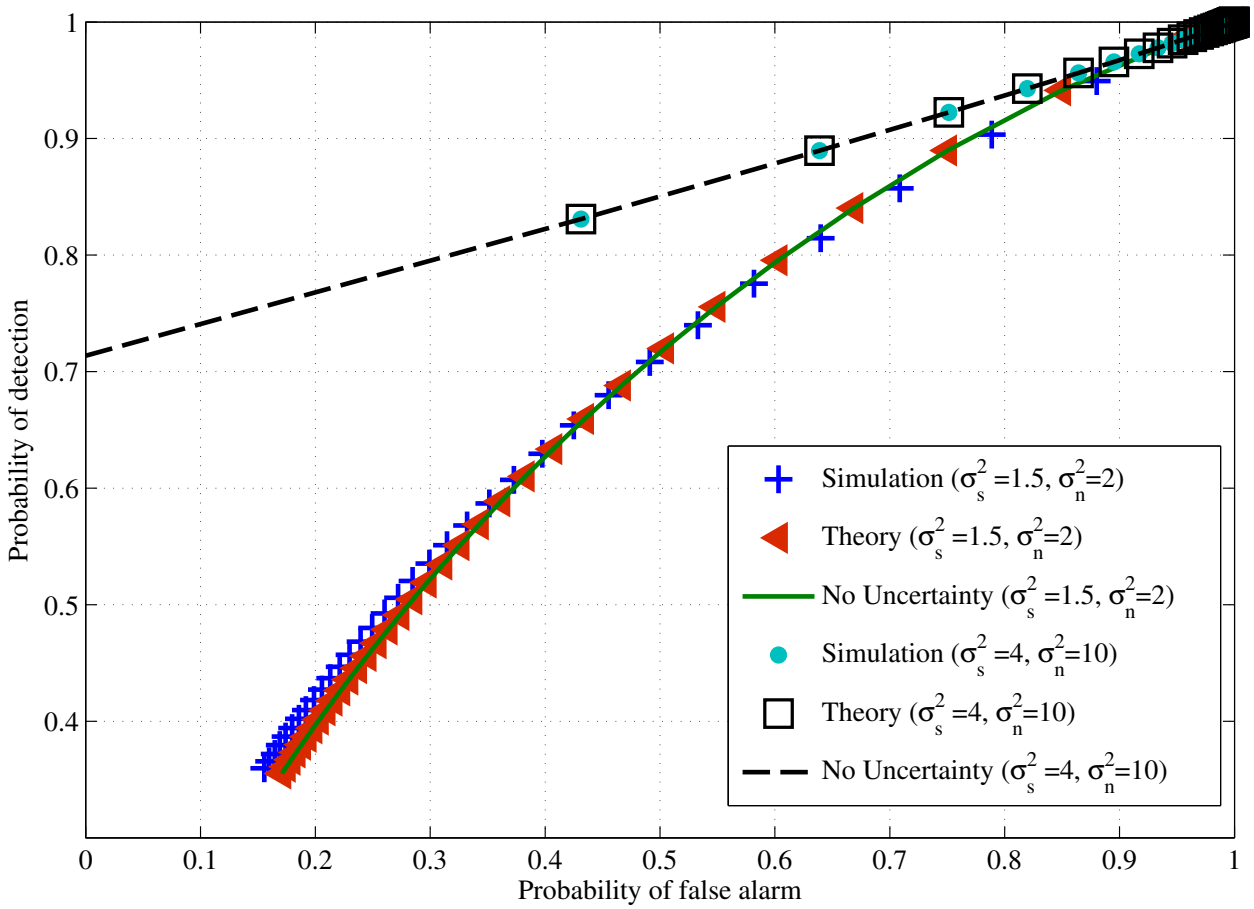

Fig. 6. Performance under noise uncertainty. ($\mathfrak{m} = 1$, $\Omega = 0.5$, $N = 3$, $M = 5$)

This article has been accepted for publication in a future issue of this journal, but has not been fully edited. Content may change prior to final publication. Citation information: DOI 10.1109/TSP.2015.2455520, IEEE Transactions on Signal Processing

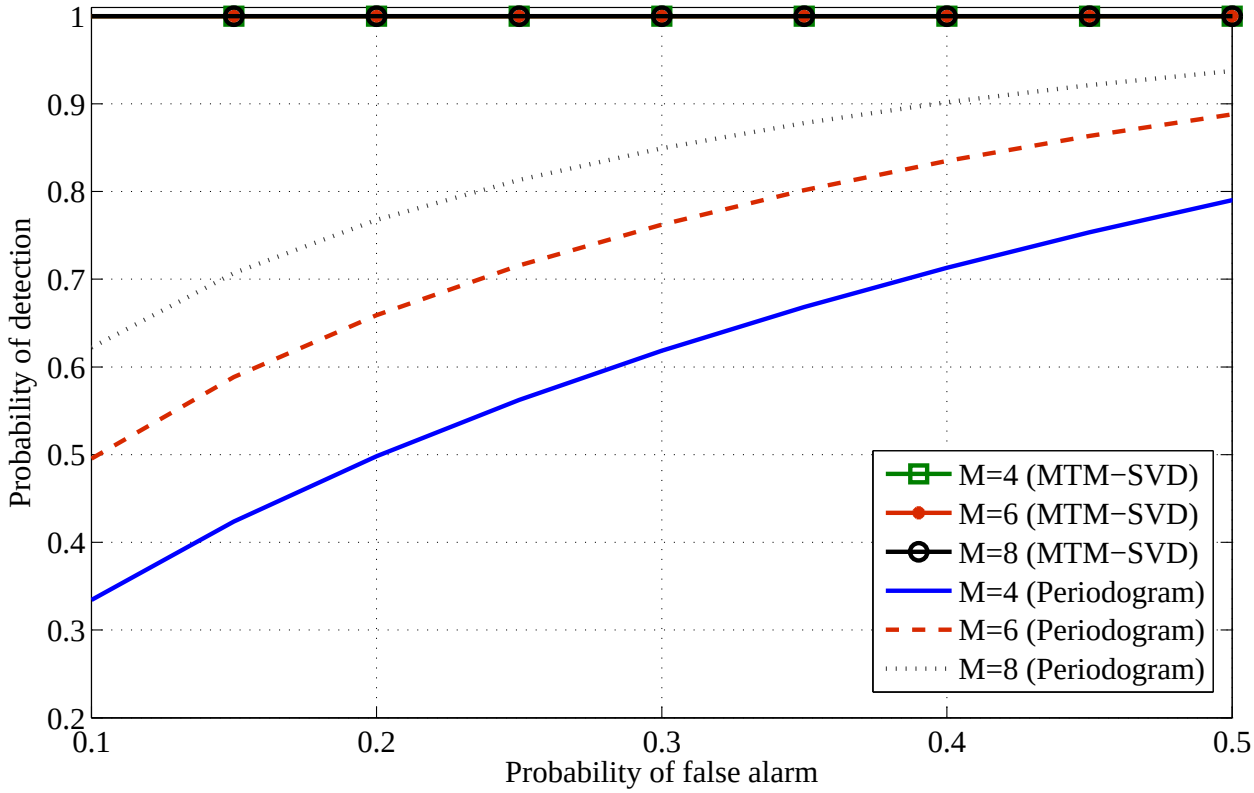

Fig. 7. Receiver operator characteristics for the MTM-SVD processor assuming i.n.i.d fading channels.

This article has been accepted for publication in a future issue of this journal, but has not been fully edited. Content may change prior to final publication. Citation information: DOI 10.1109/TSP.2015.2455520, IEEE Transactions on Signal Processing

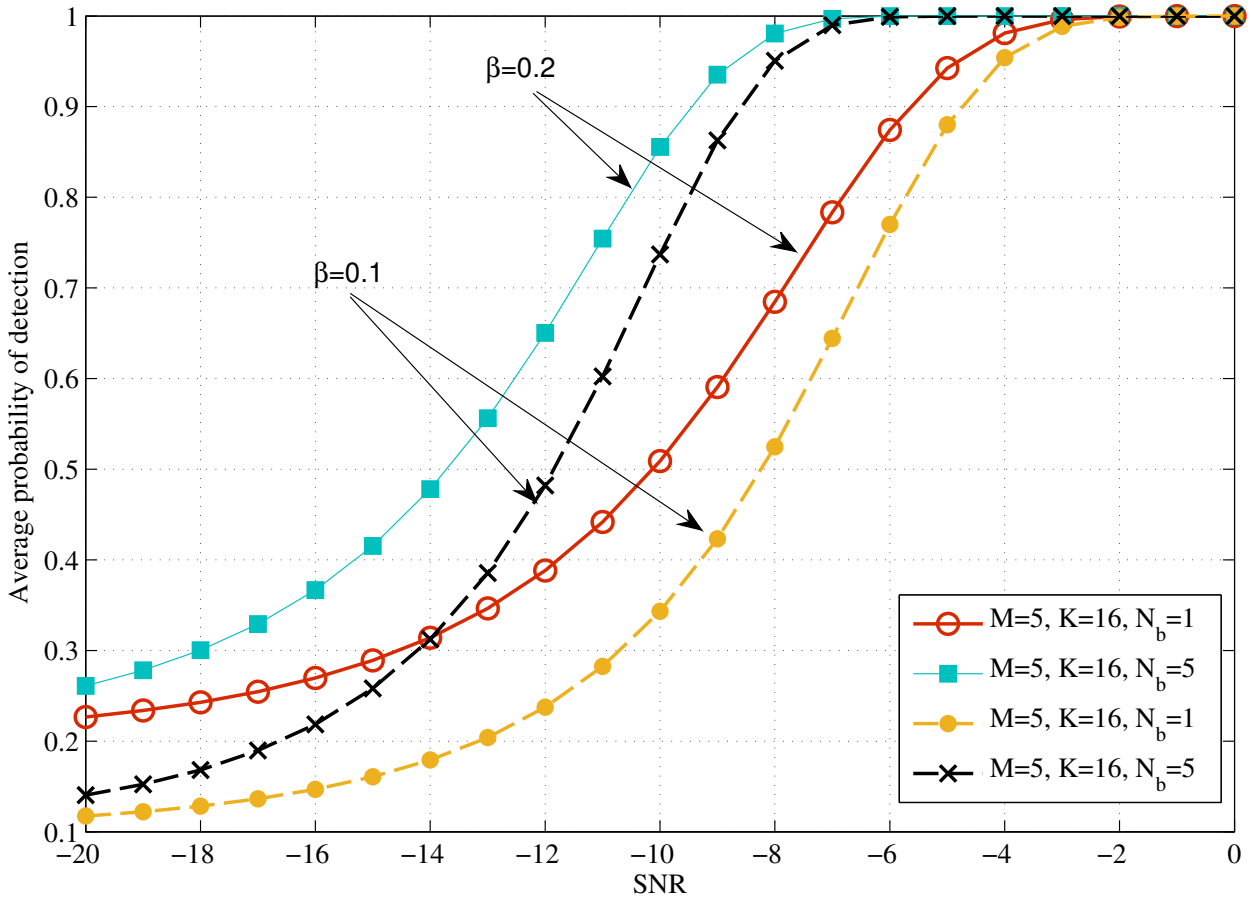

Fig. 8. Average probability of detection versus the SNR for the MTM-SVD processor.